

RESEARCH ARTICLE

# Interaction of microtubule depolymerizing agent indanocine with different human $\alpha\beta$ tubulin isotypes

Bजारंग Vasant Kumbhar, Dulal Panda, Ambarish Kunwar\*

Department of Biosciences and Bioengineering, Indian Institute of Technology Bombay, Powai, Mumbai, Maharashtra, India

\* [akunwar@iitb.ac.in](mailto:akunwar@iitb.ac.in)



**OPEN ACCESS**

**Citation:** Kumbhar BV, Panda D, Kunwar A (2018) Interaction of microtubule depolymerizing agent indanocine with different human  $\alpha\beta$  tubulin isotypes. PLoS ONE 13(3): e0194934. <https://doi.org/10.1371/journal.pone.0194934>

**Editor:** Yaakov Koby Levy, Weizmann Institute of Science, ISRAEL

**Received:** November 17, 2017

**Accepted:** March 13, 2018

**Published:** March 27, 2018

**Copyright:** © 2018 Kumbhar et al. This is an open access article distributed under the terms of the [Creative Commons Attribution License](https://creativecommons.org/licenses/by/4.0/), which permits unrestricted use, distribution, and reproduction in any medium, provided the original author and source are credited.

**Data Availability Statement:** All relevant data are within the paper and its Supporting Information files.

**Funding:** BVK is thankful to Indian Institute of Technology Bombay for Post Doctoral Fellowship. DP is thankful for the Tata Innovation Fellowship from the Department of Biotechnology, Government of India. AK is supported by Pilot Project Grants, Program for young investigators in cancer biology (Grant No. 6242-P12/RGCB/PMD/DBT/AMBK/2015) from the Department of Biotechnology, Government of India. The funders

## Abstract

Tubulin isotypes are known to regulate the stability and dynamics of microtubules, and are also involved in the development of resistance against microtubule-targeted cancer drugs. Indanocine, a potent microtubule depolymerizing agent, is highly active against multidrug-resistant (MDR) cancer cells without affecting normal cells. It is known to disrupt microtubule dynamics in cells and induce apoptotic cell death. Indanocine is reported to bind to tubulin at the colchicine site i.e. at the interface of  $\alpha\beta$  tubulin heterodimer. However, its precise binding mode, involved molecular interactions and the binding affinities with different  $\alpha\beta$ -tubulin isotypes present in MDR cells are not well understood. Here, the binding affinities of human  $\alpha\beta$ -tubulin isotypes with indanocine were examined, employing the molecular modeling approach i.e. docking, molecular dynamics simulation and binding energy calculations. Multiple sequence analysis suggests that the amino acid sequences are different in the indanocine binding pockets of  $\beta$ I,  $\beta$ IIa,  $\beta$ III and  $\beta$ VI isotypes. However, such differences are not observed in the amino acid sequences of  $\beta$ IVa,  $\beta$ IVb, and  $\beta$ V tubulin isotypes at indanocine binding pockets. Docking and molecular dynamics simulation results show that indanocine prefers the interface binding pocket of  $\alpha\beta$ IIa,  $\alpha\beta$ III,  $\alpha\beta$ IVb,  $\alpha\beta$ V, and  $\alpha\beta$ VI tubulin isotypes; whereas it is expelled from the interface binding pocket of  $\alpha\beta$ IVa and  $\alpha\beta$ I-tubulin isotypes. Further, binding free energy calculations show that  $\alpha\beta$ VI has the highest binding affinity and  $\alpha\beta$ I has the lowest binding affinity for indanocine among all  $\beta$ -tubulin isotypes. The binding free energy decreases in the order of  $\alpha\beta$ VI >  $\alpha\beta$ IVb >  $\alpha\beta$ IIa >  $\alpha\beta$ III >  $\alpha\beta$ V >  $\alpha\beta$ IVa >  $\alpha\beta$ I. Thus, our study provides a significant understanding of involved molecular interactions of indanocine with tubulin isotypes, which may help to design potent indanocine analogues for specific tubulin isotypes in MDR cells in future.

## Introduction

Microtubules are dynamic cytoskeleton filamentous proteins; they play essential roles in cell division, cell movement, and intracellular transport [1]. They are polymers of  $\alpha/\beta$ -tubulin heterodimers. These  $\alpha/\beta$ -tubulin are encoded by multiple genes which are expressed tissue-

had no role in study design, data collection and analysis, decision to publish, or preparation of the manuscript.

**Competing interests:** The authors have declared that no competing interests exist.

specifically e.g.  $\beta$ I is ubiquitous,  $\beta$ III is expressed in neuronal and testicular cells,  $\beta$ IVa in neuronal and glial cells,  $\beta$ VI is observed in the erythroid cells and platelets etc. [2,3]. In humans, ten  $\beta$ -tubulin and seven  $\alpha$ -tubulin isotypes exist [4,5] and these isotypes show considerable difference at the C-terminal end. Tubulin isotypes composition plays an essential role in regulating microtubule dynamics [6–8]. The essential roles of microtubules during the cell division make them important and attractive targets to design new anticancer agents. Anticancer agents are generally classified into microtubule stabilizing agents (MSA) and microtubule destabilizing agents (MDA). The MSAs prefer to bind at the ‘taxol site’ (e.g. paclitaxel, epothilone) whereas MDAs prefer to bind at the ‘colchicine’ and ‘vinca’ site (e.g. colchicine, indanocine, vinblastine), leading to cell death due to apoptosis in both the cases [5].

A major difficulty with the effectiveness of microtubule-targeting agents arises from the emergence of drug resistance, which is mainly due to the mutation in  $\beta$ -tubulin protein and an increased expression of the P-glycoprotein pump [9]. In addition, an over-expression of  $\beta$ -tubulin isotypes in cancerous cells also plays a crucial role in drug resistance, as they show lesser binding affinities for numerous anti-mitotic agents [10–13]. Different tubulin isotypes are overexpressed in cancerous cells; particularly overexpression  $\beta$ I,  $\beta$ II,  $\beta$ III,  $\beta$ IV, and  $\beta$ V-tubulin isotypes are associated with multidrug-resistant cancer [14–17]. Furthermore, it has also been observed that  $\beta$ II,  $\beta$ III and  $\beta$ IV tubulin isotypes show differential binding affinities for a variety of anticancer drugs e.g. taxol, colchicine, DAMA-colchicine, and nocodazole [10,12,13,18]. Therefore, these drug-resistant tubulin isotypes have been highlighted as interesting targets for designing new anticancer agents.

Indanocine, a synthetic indanone, is a microtubule depolymerizing agent with potent anti-proliferative activity [19]. Indanocine acts against multidrug-resistant (MDR) cancer cells and kills non-dividing and quiescent cells [19], but it does not affect the normal non-proliferating cells. Indanocine affects the microtubule dynamicity at very low concentration and inhibits the migration of metastatic cancer cells [20]. It prefers to bind at the interface of  $\alpha\beta$  tubulin heterodimer i.e. at the colchicine binding site [21]. Indanocine is a flexible molecule in which the indanone group and the dimethylphenol group are connected by a single bond (Fig 1B).

Indanocine binds to the  $\alpha\beta$  tubulin heterodimer in a reversible manner, and it binds to tubulin at a faster rate than colchicine [21]. Indanocine is a potent microtubule de-polymerizing agent and it acts against multidrug-resistant (MDR) cancer cells without affecting the normal cells. However, its precise binding mode involved molecular interactions and the binding affinities with different  $\alpha\beta$ -tubulin isotypes present in MDR cells are not well understood. Here, the binding affinities of human  $\alpha\beta$ -tubulin isotypes with indanocine were examined, employing molecular modeling approach.

## Computational methodology

### Sequence analysis of $\beta$ tubulin isotypes

The amino acid sequences of seven different human  $\beta$ -tubulin isotypes were taken from the UniProt database. The UniProt IDs of these  $\beta$ -tubulin sequences are as follows  $\beta$ I(Q9H4B7),  $\beta$ IIa(Q13885),  $\beta$ III(Q13509),  $\beta$ IVa(P04350),  $\beta$ IVb(P68371),  $\beta$ V(P07437), and  $\beta$ VI(Q9BUF5). To the best of our knowledge, structures of human tubulin isotypes bound with indanocine have not been determined using either X-Ray Crystallography or NMR techniques. Hence, the crystal structure of  $\alpha\beta$ -tubulin heterodimer (1SA0.pdb) from Protein Database was used as a template or reference. Bovine 1SA0.pdb has the  $\beta$ II tubulin which is identical in sequence to human  $\beta$ II tubulin [10]. Therefore, crystal structure 1SA0.pdb was used as a template to build the 3D model of human tubulin isotypes. The sequence alignments of seven different human

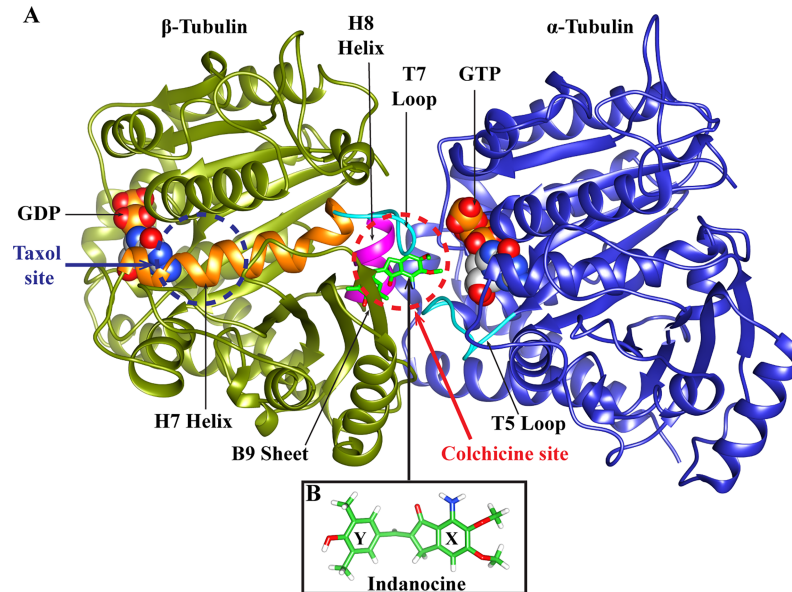


**Fig 1. The representative structure of  $\alpha\beta$ -tubulin dimer and indanocine.** (A)  $\alpha/\beta$ -tubulin subunits.  $\alpha$  subunit is shown in blue color and  $\beta$  subunit is shown in olive green color. Indanocine binding site i.e. 'colchicine site' is at the interface of  $\alpha$ -tubulin and  $\beta$ -tubulin heterodimer (red dotted circle); while the 'taxol site' is present on only  $\beta$ -tubulin over the H7 helix (blue dotted circle). The indanocine binding pocket consists of H7 helix (shown in orange), T7 loop (shown in cyan), H8 helix (shown in magenta) and T5 loop of  $\alpha$ -tubulin (shown in cyan). Here, H7 denotes the  $\alpha$ -helix number 7, T7 stands for T loop number 7, and B9 implies the  $\beta$ -sheet number 9. The GTP in  $\alpha$ -tubulin, GDP in  $\beta$ -tubulin are shown using space-fill models. The white, grey, red, blue and golden yellow colors represent carbon, hydrogen, oxygen, nitrogen and phosphorous atoms, respectively. (B) The structure of indanocine has a dimethoxyaniline group (labeled as X ring) and a dimethylphenol group (labeled as Y ring). The carbon, oxygen, nitrogen, and hydrogen atoms of indanocine are shown in green, red, blue and white color, respectively.

<https://doi.org/10.1371/journal.pone.0194934.g001>

$\beta$ -tubulin isotypes and the template sequence were performed to pinpoint the difference in residues at the indanocine binding pocket using Clustal Omega tool of EMBL-EBI [22].

### Homology modeling of human $\alpha\beta$ -tubulin isotypes

In this study, the colchicine-bound crystal structure of  $\alpha\beta$ -tubulin heterodimer (source code:1SA0.pdb) [23] was used as the template structure to build the 3D structures of seven human tubulin isotypes using homology modeling technique. Here, word template implies an initial structure used to build the desired model structure in the absence of required crystal structure, using homology modeling approach. The crystal structure of  $\alpha\beta$ -tubulin heterodimer '1SA0.pdb' is from bovine source with a resolution of 3.58Å [23]. Previously, we have shown that human  $\beta$ IIa,  $\beta$ III,  $\beta$ IVa are identical i.e. 100% similar to bovine  $\beta$ IIa,  $\beta$ III, and  $\beta$ IVa [10]. Similarly, we have also checked the similarity between other tubulin isotypes, and have found that the human  $\beta$ IVb,  $\beta$ V, and  $\beta$ VI are also identical i.e. 100% similar to bovine  $\beta$ IVb (Q3MHM5),  $\beta$ V(Q2KJD0),  $\beta$ VI(Q2HJ81) whereas human  $\beta$ I and bovine  $\beta$ I (E1BJK2) show 88.89% similarity.

We considered chains A and B from the crystal structure 1SA0.pdb for homology modeling whose missing residues of  $\beta$ -tubulin (37 to 47) and  $\alpha$ -tubulin (1, 275–284) were built using MODELLER9v18 [24]. This refined structure of  $\alpha\beta$ -tubulin heterodimers obtained from MODELLER9v18 was used as template and will be referred to as tubulin 1SA0 hereafter. The homology models of seven human  $\alpha\beta$ -tubulin isotype heterodimers such as  $\alpha\beta$ I,  $\alpha\beta$ IIa,  $\alpha\beta$ III,  $\alpha\beta$ IVa,  $\alpha\beta$ IVb,  $\alpha\beta$ V, and  $\alpha\beta$ VI were built using the template structure 1SA0.pdb through

MODELLER9v18 and the best models were selected on the basis of their DOPE score [24]. The C-terminal ends of tubulin isotypes were not included in our study as they are not present at the interface of  $\alpha\beta$ -tubulin. Therefore, we do not expect C-terminal tails to play a direct role in drug binding at the interface. C-terminal ends of the different isotypes have been modeled by Luchko et al. [25] for conformational analysis. A recent study of interaction of different human tubulin isotypes with drug DAMA-Colchicine [10] shows that C-terminal end does not qualitatively affect the binding of DAMA-Colchicine with tubulin isotypes. The stereochemical quality of  $\alpha\beta$ -tubulin models was evaluated using PROCHECK [26] and Verify-3D [27] to ensure the reliability of the homology models, whose details are given in the Supplementary S1 Text. Subsequent energy minimization was performed on tubulin 1SA0 and seven different  $\alpha\beta$ -tubulin isotype heterodimers using 5,000 steps of steepest descent method; out of which 3,000 steps were of conjugate gradient method using AMBER12 software [28]. For energy minimization, the parameters of guanosine triphosphate (GTP), and guanosine diphosphate (GDP) and  $Mg^{2+}$  were obtained from the AMBER database [29,30]. These energy minimized structures of  $\alpha\beta$ -tubulin isotypes were then used for the docking of indanocine using AutoDock4.2 [31].

In this study, we kept the  $\alpha$ -tubulin as constant and varied the beta-tubulin isotypes as accurate combinations of different  $\alpha\beta$ -tubulin isotypes is not well known experimentally. Indanocine works on various multi-drug resistant cancer cell types where over-expression of different beta-tubulin isotypes (as compared to the  $\alpha$ -tubulin isotypes) leads to drug-resistance. Hence, we did not use all possible combinations of different  $\alpha\beta$ -tubulin isotypes in this study.

### Molecular docking of indanocine with $\alpha\beta$ -tubulin isotypes

To identify the interactions of tubulin 1SA0 and different human  $\alpha\beta$ -tubulin isotypes with indanocine, molecular docking was performed using AutoDock4.2 [31]. For molecular docking, energy-minimized 3D atomic coordinates of indanocine were generated using the PRODRG server [32]. Since indanocine was suggested to bind at the interface of  $\alpha\beta$  tubulin [21], an autogrid was used to outline the putative binding pocket around the interface of  $\alpha\beta$  tubulin [31]. The Gasteiger charges were added to  $\alpha\beta$  tubulin using AutoDock4.2 [31]. Here, we used local docking methodology to delineate the binding mode of indanocine with tubulin [33,34].

A grid box of size  $60\text{\AA}\times 60\text{\AA}\times 60\text{\AA}$  with a spacing of  $0.375\text{\AA}$  was prepared at the  $\alpha\beta$  tubulin interface i.e. the putative indanocine binding site. The Lamarckian Genetic Algorithm (LGA) was used for molecular docking with default parameters [31]. Here, a total of 50 independent flexible ligand dockings were conducted, each composed of 100 LGA runs, which yielded a total of 5,000 conformations. They were subsequently clustered using an all-atom RMSD cut-off of  $4\text{\AA}$ ; which were then analyzed considering cluster size and binding free energy calculated by a scoring function of AutoDock4.2 [31,35]. The lowest binding free energy docked conformation of indanocine was selected for further hydrogen bonding interactions analysis and for molecular dynamics simulations.

### Molecular dynamics simulation

Molecular dynamics simulations were performed for indanocine-docked complexes with tubulin 1SA0 and seven different human  $\alpha\beta$  tubulin isotypes i.e.  $\alpha\beta$ I,  $\alpha\beta$ IIa,  $\alpha\beta$ III,  $\alpha\beta$ IVa,  $\alpha\beta$ IVb,  $\alpha\beta$ V,  $\alpha\beta$ VI, and  $\alpha\beta$ VII using the SANDER module of AMBER12 [28]. The AMBER ff99SB force field was applied for protein, and the parameters for guanosine triphosphate (GTP), guanosine diphosphate (GDP) and  $Mg^{2+}$  were taken from the AMBER database [29,30]. Parameters for indanocine were generated by using the 'Antechamber' module of

AMBER12 [10,36]. The implicit 'Generalized Born/Surface Area (GB/SA)' model was used to represent the solvent effect by using the parameters described by Tsui [37] to explore the interactions of protein-ligand [10,36]. The molecular dynamics simulation steps such as minimization, heating, equilibration and production run were performed using the same parameters as in our earlier studies [10]. The trajectories of molecular dynamics simulations were visualized and analyzed using VMD [38] and PyMol [39]. VMD was employed to produce the molecular dynamics simulation movies by setting the Trajectory Smoothing Window size for protein to 5, and for GTP, GDP and indanocine to 3.

### Binding energy calculations

The  $\alpha\beta$  tubulin isotype-indanocine binding free energy calculations were estimated using MM-GBSA approaches using AMBER12 [28]. The binding free energy was calculated using 10,000 frames from the last 2ns of molecular dynamics trajectories with an interval of 5 for each system using mmpbsa module of AMBER12 similar to our earlier study [10]. The entropy calculations are computationally expensive and hence omitted in this study, as done in an earlier study [10]. The need of explicit calculation of the entropy can be avoided in this study as we are comparing the relative trend of binding free energies of different isotypes which are related systems (there is a difference of few residues among them) [10,40].

## Results and discussion

### Sequence analysis and homology modeling of $\alpha\beta$ -tubulin isotypes

Multiple sequence analysis of the seven above-mentioned different human  $\beta$ -tubulin isotypes against bovine  $\beta_{II}$  tubulin (PDB code: 1SA0, chain B) as reference sequence was performed using Clustal Omega tools of EMBL-EBI [22]. The multiple sequence analysis study shows that human  $\beta$ -tubulin isotypes show residue composition variations at different locations (Fig 2). We further analyzed the residue composition variations at the indanocine binding pocket of different  $\beta$ -tubulin isotypes. The indanocine binding pocket of  $\beta I$  has five residue changes i.e. Val236-Ile, Cys239-Ser, Ala315-Cys, Val316-Ile, and Thr351-Val,  $\beta IIa$  has a single amino acid change i.e. Val316-Ile,  $\beta III$  has three residue changes i.e. Cys239-Ser, Ala315-Thr, and Thr351-Val (Fig 2), and  $\beta VI$  also has three residue changes similar to  $\beta III$  tubulin isotypes such as Cys239-Ser, Ala315-Thr, and Thr351-Val. There is no residue composition variation in  $\beta IVa$ ,  $\beta IVb$ , and  $\beta V$  at the indanocine binding pocket (Fig 2). We then built homology models of these seven human  $\alpha\beta$ -tubulin isotypes and performed molecular docking of indanocine and molecular dynamics simulations of  $\alpha\beta$  tubulin-indanocine complexes to explore the effect of residue composition on the binding interaction of indanocine.

### Molecular docking of indanocine with $\alpha\beta$ -tubulin isotypes

The binding mode and interactions of indanocine with tubulin 1SA0 and seven different human  $\alpha\beta$ -tubulin isotypes were examined by molecular docking studies (Fig 3A–3H). In different  $\alpha\beta$ -tubulin isotypes, indanocine prefers to bind at the  $\alpha\beta$ -tubulin interface binding pocket i.e. colchicine binding site (Fig 3A–3H). In all the  $\alpha\beta$ -tubulin isotypes-indanocine complexes, the dimethylphenol group is immersed inside the binding pocket of  $\beta$ -tubulin, while the dimethoxyaniline group of indanocine is located at the interface cavity of  $\alpha\beta$ -tubulin (Fig 3A–3H). This dimethoxyaniline group of indanocine forms hydrogen bonding interactions with both the residues of  $\alpha$ -tubulin and  $\beta$ -tubulin (Table 1). The lowest binding energy docked conformations of indanocine are shown in (Fig 3A–3H). Indanocine shows differences in binding conformations and energy with respect to the residue composition variations in and

CLUSTAL O(1.2.4) multiple sequence alignment

1SA0: B   PDBID   CHAIN   SEQUENCE	MREIVHIQAGQCNGIQGAKFWEVISDEHGIDPTGSHGSDQLQLERINVVYNEAAGNKVY	60
sp   Q9H4B7   TBB1_HUMAN	MREIVHIQIGQCNGIQGAKFWEVIGEEHGIDLAGSDRGASALQLERISVYVYNEAYGRKYV	60
sp   Q13885   TBB2A_HUMAN	MREIVHIQAGQCNGIQGAKFWEVISDEHGIDPTGSHGSDQLQLERINVVYNEAAGNKVY	60
sp   Q13509   TBB3_HUMAN	MREIVHIQAGQCNGIQGAKFWEVISDEHGIDPDSGNVYVGDSDQLQLERISVYVYNEASSHKYV	60
sp   P04350   TBB4A_HUMAN	MREIVHLQAGQCNGIQGAKFWEVISDEHGIDPTGTYHGSDQLQLERINVVYNEATGGNYV	60
sp   P68371   TBB4B_HUMAN	MREIVHLQAGQCNGIQGAKFWEVISDEHGIDPTGTYHGSDQLQLERINVVYNEATGGKYV	60
sp   P07437   TBB5_HUMAN	MREIVHIQAGQCNGIQGAKFWEVISDEHGIDPTGTYHGSDQLQLDRISVYVYNEATGGKYV	60
sp   Q9BUF5   TBB6_HUMAN	MREIVHIQAGQCNGIGTKFWEVISDEHGIDPAGGYVGDSDALQLERINVVYNESSQKYV	60
	*****: * *****:****: * :***** : * * * * * : * * * * * : * : * * *	
1SA0: B   PDBID   CHAIN   SEQUENCE	PRAILVDLEPGTMDSVRSRGGPFQIFRPDNFVFGQSGAGNNWAKGHYTEGAELVDSVLDV	120
sp   Q9H4B7   TBB1_HUMAN	PRAVLVDLEPGTMDSVRSRSGKLGALFQPSDFVHGNSGAGNNWAKGHYTEGAELIENVLEVV	120
sp   Q13885   TBB2A_HUMAN	PRAILVDLEPGTMDSVRSRGGPFQIFRPDNFVFGQSGAGNNWAKGHYTEGAELVDSVLDV	120
sp   Q13509   TBB3_HUMAN	PRAILVDLEPGTMDSVRSRGAHGLFRPDPNFVFGQSGAGNNWAKGHYTEGAELVDSVLDV	120
sp   P04350   TBB4A_HUMAN	PRAVLVDLEPGTMDSVRSRGGPFQIFRPDNFVFGQSGAGNNWAKGHYTEGAELVDAVLDV	120
sp   P68371   TBB4B_HUMAN	PRAVLVDLEPGTMDSVRSRGGPFQIFRPDNFVFGQSGAGNNWAKGHYTEGAELVDSVLDV	120
sp   P07437   TBB5_HUMAN	PRAILVDLEPGTMDSVRSRGGPFQIFRPDPNFVFGQSGAGNNWAKGHYTEGAELVDSVLDV	120
sp   Q9BUF5   TBB6_HUMAN	PRALVDLEPGTMDSVRSRGGPQLFRPDPNFVFGQSGAGNNWAKGHYTEGAELVDAVLDV	120
	*****: * * * * * : * * * * * : * * * * * : * * * * * : * * * * * : * * * * *	
1SA0: B   PDBID   CHAIN   SEQUENCE	RKESCDCLQGFQLTHSLGGGTSGMGTLTISKIREEYPDRIMNTFSVVPSPKVSOTV	180
sp   Q9H4B7   TBB1_HUMAN	RHESECDCLQGFQIVHSLGGGTSGMGTLTINMKIREEYPDRIMNFSVVPSPKVSOTV	180
sp   Q13885   TBB2A_HUMAN	RKESCDCLQGFQLTHSLGGGTSGMGTLTISKIREEYPDRIMNTFSVVPSPKVSOTV	180
sp   Q13509   TBB3_HUMAN	RKCECNDCLQGFQLTHSLGGGTSGMGTLTISKVIREEYPDRIMNTFSVVPSPKVSOTV	180
sp   P04350   TBB4A_HUMAN	RKEAESCDCLQGFQLTHSLGGGTSGMGTLTISKIREEYPDRIMNTFSVVPSPKVSOTV	180
sp   P68371   TBB4B_HUMAN	RKEAESCDCLQGFQLTHSLGGGTSGMGTLTISKIREEYPDRIMNTFSVVPSPKVSOTV	180
sp   P07437   TBB5_HUMAN	RKEAESCDCLQGFQLTHSLGGGTSGMGTLTISKIREEYPDRIMNTFSVVPSPKVSOTV	180
sp   Q9BUF5   TBB6_HUMAN	RKECEHCDCLQGFQLTHSLGGGTSGMGTLTISKIREEYPDRIMNTFSVVPSPKVSOTV	180
	* * * * * : * * * * * : * * * * * : * * * * * : * * * * * : * * * * * : * * * * *	
1SA0: B   PDBID   CHAIN   SEQUENCE	EPYNATLSVHQLVENTDETYCIDNEALYDLCFRTLKLTTPTYGDLNHLVATMSGVTTC	240
sp   Q9H4B7   TBB1_HUMAN	EPYNAVLSIHQLIENADACFCIDNEALYDLCFRTLKLTTPTYGDLNHLVATMSGVTTC	240
sp   Q13885   TBB2A_HUMAN	EPYNATLSVHQLVENTDETYCIDNEALYDLCFRTLKLTTPTYGDLNHLVATMSGVTTC	240
sp   Q13509   TBB3_HUMAN	EPYNATLSIHQLVENTDETYCIDNEALYDLCFRTLKLTATPTTYGDLNHLVATMSGVTTC	240
sp   P04350   TBB4A_HUMAN	EPYNATLSVHQLVENTDETYCIDNEALYDLCFRTLKLTTPTYGDLNHLVATMSGVTTC	240
sp   P68371   TBB4B_HUMAN	EPYNATLSVHQLVENTDETYCIDNEALYDLCFRTLKLTTPTYGDLNHLVATMSGVTTC	240
sp   P07437   TBB5_HUMAN	EPYNATLSVHQLVENTDETYCIDNEALYDLCFRTLKLTTPTYGDLNHLVATMSGVTTC	240
sp   Q9BUF5   TBB6_HUMAN	EPYNATLSVHQLVENTDETYCIDNEALYDLCFRTLKLTTPTYGDLNHLVATMSGVTTC	240
	*****: * * * * * : * * * * * : * * * * * : * * * * * : * * * * * : * * * * *	
1SA0: B   PDBID   CHAIN   SEQUENCE	RFPGQLNADLRKLVANMVPFRLHFMPGFAPLTSRGSQQYRALVPPELTQQMFDARNMM	300
sp   Q9H4B7   TBB1_HUMAN	RFPGQLNADLRKLVANMVPFRLHFMPGFAPLTAQGSQQYRALVSAELTQQMFDARNMM	300
sp   Q13885   TBB2A_HUMAN	RFPGQLNADLRKLVANMVPFRLHFMPGFAPLTSRGSQQYRALVPPELTQQMFDARNMM	300
sp   Q13509   TBB3_HUMAN	RFPGQLNADLRKLVANMVPFRLHFMPGFAPLTSRGSQQYRALVPPELTQQMFDARNMM	300
sp   P04350   TBB4A_HUMAN	RFPGQLNADLRKLVANMVPFRLHFMPGFAPLTSRGSQQYRALVPPELTQQMFDARNMM	300
sp   P68371   TBB4B_HUMAN	RFPGQLNADLRKLVANMVPFRLHFMPGFAPLTSRGSQQYRALVPPELTQQMFDARNMM	300
sp   P07437   TBB5_HUMAN	RFPGQLNADLRKLVANMVPFRLHFMPGFAPLTSRGSQQYRALVPPELTQQMFDARNMM	300
sp   Q9BUF5   TBB6_HUMAN	RFPGQLNADLRKLVANMVPFRLHFMPGFAPLTSRGSQQYRALVPPELTQQMFDARNMM	300
	*****: * * * * * : * * * * * : * * * * * : * * * * * : * * * * * : * * * * *	
1SA0: B   PDBID   CHAIN   SEQUENCE	AACDRHRGRLTVA <sup>AV</sup> FRGRMSMKEVDEQMLNVQNKNSYFVEWIPNNVK <sup>TA</sup> AVCDIPPRG	360
sp   Q9H4B7   TBB1_HUMAN	AACDLRRGRYLTVA <sup>CI</sup> FRGMSTKEVDQQLLSVQTRNSSCFVEWIPNNVK <sup>VA</sup> AVCDIPPRG	360
sp   Q13885   TBB2A_HUMAN	AACDRHRGRLTVA <sup>AI</sup> FRGRMSMKEVDEQMLNVQNKNSYFVEWIPNNVK <sup>TA</sup> AVCDIPPRG	360
sp   Q13509   TBB3_HUMAN	AACDRHRGRLTVA <sup>TV</sup> FRGRMSMKEVDEQMLAIQSKNSYFVEWIPNNVK <sup>VA</sup> AVCDIPPRG	360
sp   P04350   TBB4A_HUMAN	AACDRHRGRLTVA <sup>AV</sup> FRGRMSMKEVDEQMLSVQSKNSYFVEWIPNNVK <sup>TA</sup> AVCDIPPRG	360
sp   P68371   TBB4B_HUMAN	AACDRHRGRLTVA <sup>AV</sup> FRGRMSMKEVDEQMLNVQNKNSYFVEWIPNNVK <sup>TA</sup> AVCDIPPRG	360
sp   P07437   TBB5_HUMAN	AACDRHRGRLTVA <sup>AV</sup> FRGRMSMKEVDEQMLNVQNKNSYFVEWIPNNVK <sup>TA</sup> AVCDIPPRG	360
sp   Q9BUF5   TBB6_HUMAN	AACDRHRGRLTVA <sup>TV</sup> FRGPMMSMKEVDEQMLAIQSKNSYFVEWIPNNVK <sup>VA</sup> AVCDIPPRG	360
	**** * : * * * * * : * * * * * : * * * * * : * * * * * : * * * * * : * * * * *	
1SA0: B   PDBID   CHAIN   SEQUENCE	LKMSATFIGNSTAIQELFKRISEQFTAMFRKAF <sup>LHWY</sup> TGEGMDEMEFTEAESNMNDLVS	420
sp   Q9H4B7   TBB1_HUMAN	LSMAATFIGNNTAIQELFNRVSEHFSAMFRKAF <sup>VHWY</sup> TSGMDINEFGEAENNIHDLVS	420
sp   Q13885   TBB2A_HUMAN	LKMSATFIGNSTAIQELFKRISEQFTAMFRKAF <sup>LHWY</sup> TGEGMDEMEFTEAESNMNDLVS	420
sp   Q13509   TBB3_HUMAN	LKMSSTFIGNSTAIQELFKRISEQFTAMFRKAF <sup>LHWY</sup> TGEGMDEMEFTEAESNMNDLVS	420
sp   P04350   TBB4A_HUMAN	LKMSATFIGNSTAIQELFKRISEQFTAMFRKAF <sup>LHWY</sup> TGEGMDEMEFTEAESNMNDLVS	420
sp   P68371   TBB4B_HUMAN	LKMSATFIGNSTAIQELFKRISEQFTAMFRKAF <sup>LHWY</sup> TGEGMDEMEFTEAESNMNDLVS	420
sp   P07437   TBB5_HUMAN	LKMAVTFIGNSTAIQELFKRISEQFTAMFRKAF <sup>LHWY</sup> TGEGMDEMEFTEAESNMNDLVS	420
sp   Q9BUF5   TBB6_HUMAN	LKMASTFIGNSTAIQELFKRISEQFSAMFRKAF <sup>LHWY</sup> TGEGMDEMEFTEAESNMNDLVS	420
	* * * * * : * * * * * : * * * * * : * * * * * : * * * * * : * * * * * : * * * * *	
1SA0: B   PDBID   CHAIN   SEQUENCE	EYQQYQDATADEQGEF--EEEGEEDEA----445	
sp   Q9H4B7   TBB1_HUMAN	EYQQYQDAKAVLEDEEVEEAEEMEPEDKGH-451	
sp   Q13885   TBB2A_HUMAN	EYQQYQDATADEQGEF--EEEGEEDEA----445	
sp   Q13509   TBB3_HUMAN	EYQQYQDATAEEEGEM--YEDDEEEEAQGPK450	
sp   P04350   TBB4A_HUMAN	EYQQYQDATAE-EGEF--EEEAEEVA----444	
sp   P68371   TBB4B_HUMAN	EYQQYQDATAEEEGEF--EEEAEEVA----445	
sp   P07437   TBB5_HUMAN	EYQQYQDATAEEEDF--GEEAEEEA----444	
sp   Q9BUF5   TBB6_HUMAN	EYQQYQDATAANDGEEA--FDEEEEDIG--446	
	*****: * * * * * : * * * * * : * * * * * : * * * * * : * * * * * : * * * * *	

**Fig 2. Multiple sequence alignment of human  $\beta$ -tubulin isotypes.** The isotype  $\beta$ I shows variations of residues Val236-Ile, Cys239-Ser, Ala315-Cys, Val316-Ile and Thr351-Val,  $\beta$ IIa shows a change of Val316-Ile,  $\beta$ III and  $\beta$ VI shows a change of Cys239-Ser, Ala315-Thr, and Thr351-Val at the indanocine binding pocket. Residue variations in the indanocine binding pocket are shown in red. Symbol ‘\*’ denotes positions of amino acid which have a single, fully conserved amino acid residue; the symbol ‘.’ denotes conservation between groups of strongly similar properties of amino acid; the symbol ‘:’ denotes the conservation between groups of weakly similar properties of amino acids, and the symbol ‘—’ denotes gaps inserted to maximize sequence alignment [22].

<https://doi.org/10.1371/journal.pone.0194934.g002>

around the binding pocket of different  $\alpha\beta$ -tubulin isotypes (Fig 3A–3H and Table 1). The binding energy of indanocine with tubulin 1SA0 and different  $\alpha\beta$ I,  $\alpha\beta$ IIa,  $\alpha\beta$ III,  $\alpha\beta$ IVa,

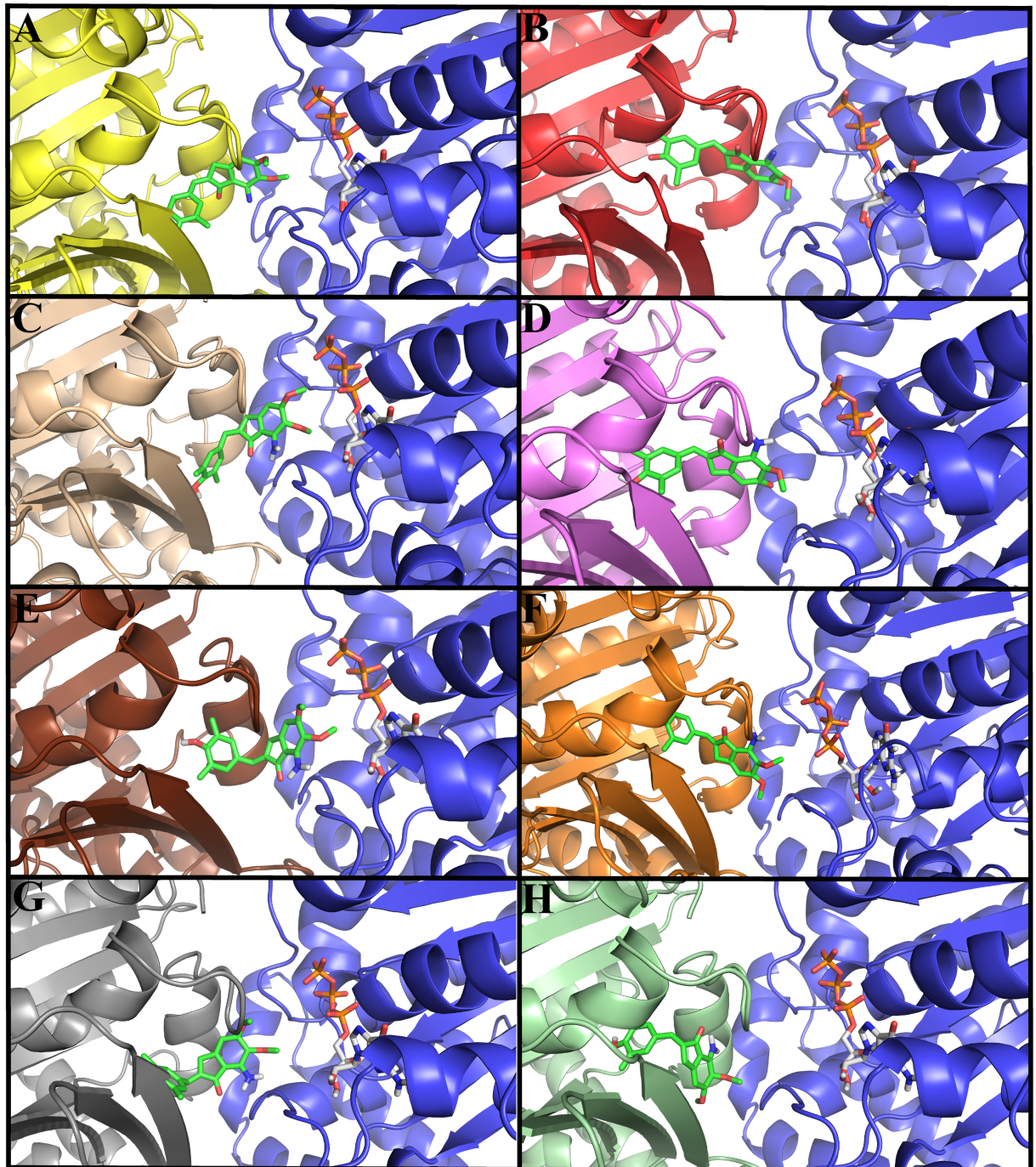


**Fig 3. Docked conformations of indanocine with  $\alpha\beta$ -tubulin isotypes.** The color for  $\alpha$ -tubulin is blue in all  $\alpha\beta$ -tubulin heterodimers while color of different  $\beta$ -tubulin isotypes is different in all  $\alpha\beta$ -tubulin heterodimers. The color code for  $\beta$ -tubulin is yellow for tubulin 1SA0, red for isotype  $\beta$ I, light brown for isotype  $\beta$ IIa, violet for isotype  $\beta$ III, chocolate for isotype  $\beta$ IVa, orange for isotype  $\beta$ IVb, grey for isotype  $\beta$ V and light green for isotype  $\beta$ VI. Here, indanocine and GTP is shown in stick model and the color code for indanocine and GTP is same as shown in Fig 1. (A) tubulin 1SA0-indanocine complex (B)  $\alpha\beta$ I tubulin isotype-indanocine complex. (C)  $\alpha\beta$ IIa tubulin isotype-indanocine complex (D)  $\alpha\beta$ III tubulin isotype-indanocine complex (E)  $\alpha\beta$ IVa tubulin isotype-indanocine complex (F)  $\alpha\beta$ IVb tubulin isotype-indanocine complex (G)  $\alpha\beta$ V tubulin isotype-indanocine complex. (H)  $\alpha\beta$ VI tubulin isotype-indanocine complex. Indanocine prefers the  $\alpha\beta$ -tubulin interface binding pocket in all human  $\alpha\beta$ -tubulin isotypes.

<https://doi.org/10.1371/journal.pone.0194934.g003>

**Table 1. Binding energy as well as interactions of indanocine with tubulin 1SA0 and different human  $\alpha\beta$  tubulin isotypes after molecular docking.**

Tubulin Isotypes	Binding energy (kcal/mol)	Hydrogen bonding interactions			Figure references
		Atoms involved	Distance (Å)	Angle (Degree)	
tubulin 1SA0	-8.09	Ala-315NH...O-Ind	2.18	132.08	Fig 3A, S9A Fig
		Lys-350CH...O-Ind	2.10	121.40	
		Thr-179-O...HN-Ind	2.16	148.31	
		Asn-101-NH...O-Ind	2.63	145.84	
$\alpha\beta$ I	-9.09	Ile-236-O...HO-Ind	2.22	103.54	Fig 3B, S9B Fig
		Leu-246-O...HN-Ind	2.00	130.95	
		Lys-252-H...N-Ind	2.54	151.14	
		Ind-O...H-Leu-246	2.14	152.37	
		Asn101-NH...O-Ind	2.92	132.15	
$\alpha\beta$ IIa	-8.07	Lys-252-NH...O-Ind	2.42	158.46	Fig 3C, S9C Fig
		Lys-350-2BH...O-Ind	1.90	173.19	
		Thr-179-O...HN-Ind	1.98	125.69	
		Asn-101-NH...O-Ind	2.88	141.62	
$\alpha\beta$ III	-8.30	Leu-246-O...HN-Ind	2.10	98.13	Fig 3D, S9D Fig
		Lys-252-N...HN-Ind	2.61	127.94	
		Tyr-169-O...HO-Ind	2.00	176.83	
$\alpha\beta$ IVa	-7.81	Cys-239-SH...O-Ind	1.84	170.83	Fig 3E, S9E Fig
		Lys-252-NH...O-Ind	2.07	167.76	
		Ser-178-O...HN_Ind	2.26	129.35	
		Ser-178-O...HN-Ind	2.20	110.70	
$\alpha\beta$ IVb	-8.73	Leu-240NH...O-Ind	2.38	126.85	Fig 3F, S9F Fig
		Val-236-O...HO-Ind	1.73	167.99	
		Cys-239-NH...O-Ind	2.90	98.70	
		Leu-246-CH...O-Ind	2.23	129.32	
		Ala-248-NH...O-Ind	2.70	107.0	
		Asn-256-HN...O-Ind	2.58	98.06	
		Ser-178-OH...O-Ind	2.19	161.91	
$\alpha\beta$ V	-8.10	Ala-315-O...HO-Ind	1.88	126.21	Fig 3G, S9G Fig
		Lys-252-CH...O-Ind	2.29	139.33	
		Asn-101-NH...O-Ind	2.17	152.54	
		Thr-179-O...HN-Ind	2.20	101.10	
$\alpha\beta$ VI	-8.85	Val-180-N...HN-Ind	2.80	123.10	Fig 3H, S9H Fig
		Tyr-169-O...HO-Ind	2.06	164.22	
		Lys-252-NH...N-Ind	1.97	123.25	
		Lys-350-CH...O-Ind	2.72	164.94	
		Asn256-N...HN-Ind	2.60	134.00	

<https://doi.org/10.1371/journal.pone.0194934.t001>

$\alpha\beta$ IVb,  $\alpha\beta$ V, and  $\alpha\beta$ VI tubulin isotypes are -8.09, -9.09, -8.07, -8.30, -7.81, -8.73, -8.10 and -8.85 kcal/mol respectively (Table 1).

The analysis of hydrogen bonding interactions of  $\alpha\beta$ -tubulin isotypes-indanocine docked complexes shows differences in the hydrogen bonding interactions within the interface binding pocket of different  $\alpha\beta$ -tubulin isotypes (Table 1). The analysis of tubulin 1SA0-indanocine complex (Fig 3A) shows that the indanocine forms hydrogen bonding interactions with residues Ala-315 (2.18Å), Lys-350 (2.10Å) of  $\beta$ -tubulin, and Thr-179 (2.16Å) and Asn-101 (2.63Å) of  $\alpha$ -tubulin (S9A Fig and Table 1). Here, Ala-315, interact with the dimethylphenol group of indanocine and Lys-350, Thr-179 and Asn-101 interact with the dimethoxyaniline group of



indanocine (S9A Fig). The analysis of  $\alpha\beta$ I-tubulin isotype-indanocine complex (Fig 3B) shows that indanocine forms hydrogen bonding interactions with the residues Ile-236(2.22Å), Leu-246(2.00Å), Leu-246(2.14Å), Lys-252 (2.54Å) of  $\beta$ -tubulin, and Asn-101(2.92Å) of T5-loop of  $\alpha$ -tubulin (S9B Fig and Table 1). Here, Ile-236 interacts with the dimethylphenol group and Leu-246, Lys-252 of  $\beta$ -tubulin and Asn-101 of  $\alpha$ -tubulin interacts with the dimethoxyaniline group of indanocine. Next, the analysis of  $\alpha\beta$ IIa-tubulin isotype-indanocine complex (Fig 3C) shows that indanocine forms hydrogen bonding interactions with Lys-252(2.42Å), and Lys-350(1.90Å) of  $\beta$ -tubulin, and with Thr-179(1.98Å) and Asn-101(2.88Å) of T5-loop of  $\alpha$ -tubulin (S9C Fig). Here, Lys-350 interacts with the dimethylphenol group of indanocine and Lys-252 of  $\beta$ -tubulin, and Thr-179 and Asn-101 of  $\alpha$ -tubulin interacts with the dimethoxyaniline group of indanocine (S9C Fig).

Further analysis of molecular docking complex of  $\alpha\beta$ III-tubulin isotype-indanocine (Fig 3D) shows that indanocine makes bonding interactions with residues Leu-246 (2.10Å), Lys-252(2.61Å) and Tyr-169(2.00Å) of  $\beta$ -tubulin (S9D Fig and Table 1). Here, Leu-246 and Lys-252 interact with the dimethoxyaniline group of indanocine and Tyr-169 interacts with a dimethylphenol group of indanocine (S9D Fig). Next, the analysis of  $\alpha\beta$ IVa-tubulin isotype-indanocine complex (Fig 3E) shows that indanocine forms hydrogen bonding interactions with residues Cys-239 (1.84Å), Lys-252 (2.07Å) of  $\beta$ -tubulin and Ser-178 (2.26Å) and Ser-178 (2.20Å) of T5-loop of  $\alpha$ -tubulin (S9E Fig and Table 1). Here, Cys-239 interacts with the dimethylphenol group, and Lys-252 and Ser-178 interact with the dimethoxyaniline group of indanocine (S9E Fig and Table 1). The analysis of  $\alpha\beta$ IVb-tubulin isotype and indanocine (Fig 3F) complex shows that indanocine forms hydrogen bonding interactions with residues Val-236 (1.73Å), Cys-239 (2.90Å), Leu-240 (2.38Å), Leu-246 (2.23Å), Ala-248(2.70Å) and Asn-256 (2.58Å) of  $\beta$ -tubulin and Ser-178 (2.19Å) of T5-loop of  $\alpha$ -tubulin (S9F Fig and Table 1). The amino acids Val-236, Cys-239, Leu-240 interact with the dimethylphenol group and Leu-246, Ala-248, Asn-256 and Ser-178 interact with the dimethoxyaniline group of indanocine (S9F Fig and Table 1). Afterwards, an analysis of the docking complex of  $\alpha\beta$ V-tubulin isotype-indanocine (Fig 3G) shows that indanocine forms hydrogen bonding interactions with residues Ala-315 (1.88Å), Lys-252 (2.29Å) of  $\beta$ -tubulin, Asn-101 (2.17Å), and Val-180 (2.80Å) and Thr-179 (2.20Å) of  $\alpha$ -tubulin. Here, Ala-315 interacts with the dimethylphenol group of indanocine which is immersed inside the binding pocket of  $\beta$ -tubulin, and Lys-252, Asn-101, Val-180, Thr-179 interact with the dimethoxyaniline group of indanocine (S9G Fig and Table 1). Finally, analysis of  $\alpha\beta$ VI-tubulin isotype and indanocine (Fig 3H) complex shows that indanocine forms interactions with residues Tyr-169 (2.06Å), Asn-256 (2.60Å), Lys350 (2.72 Å) and Lys-252 (1.97Å) of  $\beta$ -tubulin (S9H Fig and Table 1). In this complex, indanocine does not form any hydrogen bonding interactions with  $\alpha$ -tubulin. Here, Tyr-169 interacts with the dimethylphenol group and Lys-252, Asn-256 and Lys-350 with the dimethoxyaniline group of indanocine.

Molecular docking results suggest that the residue composition variation in and around the indanocine binding pocket results in differences in binding energy, conformation, and hydrogen bonding interactions among the different  $\alpha\beta$ -tubulin isotypes-indanocine complexes (Fig 3A–3H and Table 1). Thus, our docking studies suggest that Lys-252, Lys-350, Cys-239, Val-236, Ala-248, Leu-246 of  $\beta$ -tubulin and Ala-101, Ser-178, Thr-179 and Val-180 play a key role in the stabilization of indanocine at the interface of all  $\alpha\beta$ -tubulin heterodimer (S9A–S9H Fig).

Further, we calculated the electrostatic contact potential over the tubulin 1SA0 and seven different  $\beta$ -tubulin isotypes-indanocine complex using PyMol [39] (S10A–S10H Fig). The electrostatic contact potentials show that the dimethylphenol group is immersed inside the cavity of  $\beta$ -tubulin while the dimethoxyaniline group of indanocine is located out of  $\beta$ -tubulin protein. In addition, the effect of residue composition variation in and around the indanocine

binding pocket in different  $\beta$ -tubulin isotypes was further elucidated using molecular dynamics simulations and binding free energy calculations.

### Molecular dynamics simulation of $\alpha\beta$ tubulin isotypes-indanocine complexes

To understand the refined binding mode of  $\alpha\beta$ -tubulin isotypes with indanocine, we performed molecular dynamics simulations over the lowest energy  $\alpha\beta$ -tubulin-indanocine docked complexes (Fig 3A–3H) as our starting structure using AMBER12 [28]. The primary analysis was done by looking at the molecular dynamics simulation stability (Fig 4) and analysis of molecular dynamics simulated average structures (Fig 5A–5H).

The Root mean square deviations (RMSD) of C $\alpha$  backbone atoms of a production molecular dynamics simulations was calculated to examine the stability of the molecular dynamics simulation. The RMSD analysis of all the different  $\alpha\beta$ -tubulin isotypes-indanocine complexes suggests that all  $\alpha\beta$ -tubulin-indanocine complexes reached their equilibrium conformation after a time period of 20ns and then retained their stability with fluctuations between 2.5–4.5Å (Fig 4). Molecular dynamics simulation results clearly show that indanocine prefers to bind at the  $\alpha\beta$ -tubulin interface binding pocket in tubulin 1SA0 and  $\alpha\beta$ Ia,  $\alpha\beta$ III,  $\alpha\beta$ IVb,  $\alpha\beta$ V, and  $\alpha\beta$ VI tubulin isotypes (S1 Movie, S3 and S4 Movies, S6–S8 Movies) respectively, while in case of tubulin isotype  $\alpha\beta$ I (S2 Movie) and  $\alpha\beta$ IVa (S5 Movie), indanocine is expelled from the  $\alpha\beta$ -tubulin interface binding cavity. In  $\alpha\beta$ I and  $\alpha\beta$ IVa tubulin isotypes, the T7 loop of  $\beta$ -tubulin moves backward, while the B9 sheet of  $\beta$ -tubulin and T5 loop of  $\alpha$ -tubulin also undergo conformational changes which makes ample space at the interface leading to the expulsion of indanocine from the interface of  $\alpha\beta$ -tubulin isotypes heterodimer (S2 Movie and S5 Movie). Such conformational changes are seen in cases of  $\alpha\beta$ I and  $\alpha\beta$ IVa tubulin isotypes but are not seen on other tubulin isotypes (S1 Movie, S3 and S4 Movies, S6–S8 Movies). The residues present in the B9 sheet, H7 helix, T7 loop and H8 helix of  $\beta$ -tubulin and T5 loop of  $\alpha$ -tubulin have important contributions in the binding of indanocine at the interface in other  $\alpha\beta$ -tubulin isotypes (S1 Movie, S3 and S4 Movies, S6–S8 Movies). A detailed analysis of residues involved in the hydrogen bonding interactions with indanocine is discussed in the next section.

### Analysis of average structure of $\alpha\beta$ -tubulin isotypes-indanocine complex

To understand the refined binding mode and interactions of tubulin 1SA0 and different  $\alpha\beta$ -tubulin isotypes with indanocine, molecular dynamics simulated average structures were analyzed (Fig 5A–5H and Table 2). The RMSD differences of indanocine between the MD simulated ‘starting structure’ (i.e. docked structure) and ‘end structure’ were determined in tubulin 1SA0 and  $\alpha\beta$ I,  $\alpha\beta$ Ia,  $\alpha\beta$ III,  $\alpha\beta$ IVa,  $\alpha\beta$ IVb,  $\alpha\beta$ V and  $\alpha\beta$ VI tubulin isotypes. These RMSD differences were found to be 4.11Å, 13.26Å, 2.92Å, 8.98Å, 5.92Å, 6.16Å, 4.63Å and 8.38 Å for tubulin 1SA0 and  $\alpha\beta$ I,  $\alpha\beta$ Ia,  $\alpha\beta$ III,  $\alpha\beta$ IVa,  $\alpha\beta$ IVb,  $\alpha\beta$ V and  $\alpha\beta$ VI tubulin isotypes respectively. The RMSD analysis shows that indanocine largely deviates from the initial position in the  $\alpha\beta$ I tubulin isotype (Fig 5B) as compared to the other  $\alpha\beta$ -tubulin-indanocine complexes. The detailed hydrogen bonding interactions of  $\alpha\beta$ -tubulin isotypes with indanocine are listed in Table 2.

The analysis of tubulin 1SA0-indanocine complex (Fig 5A) shows that indanocine makes hydrogen bonding interactions with residue Cys-239(3.00Å), Lys-350(2.28Å), Lys-252 (2.77Å), and Asn-256 (2.82Å) of  $\beta$ -tubulin and Asn-101(2.91Å) and Thr-179(1.86Å) of  $\alpha$ -tubulin Table 2. Here, Lys-350, Asn-256, Lys-252, Asn-101, and Thr-179 interact with the dimethoxyaniline group of indanocine and only Cys-239 interacts with the dimethylphenol group of indanocine (S11A Fig). Analysis of the average structure of  $\alpha\beta$ I tubulin isotype-

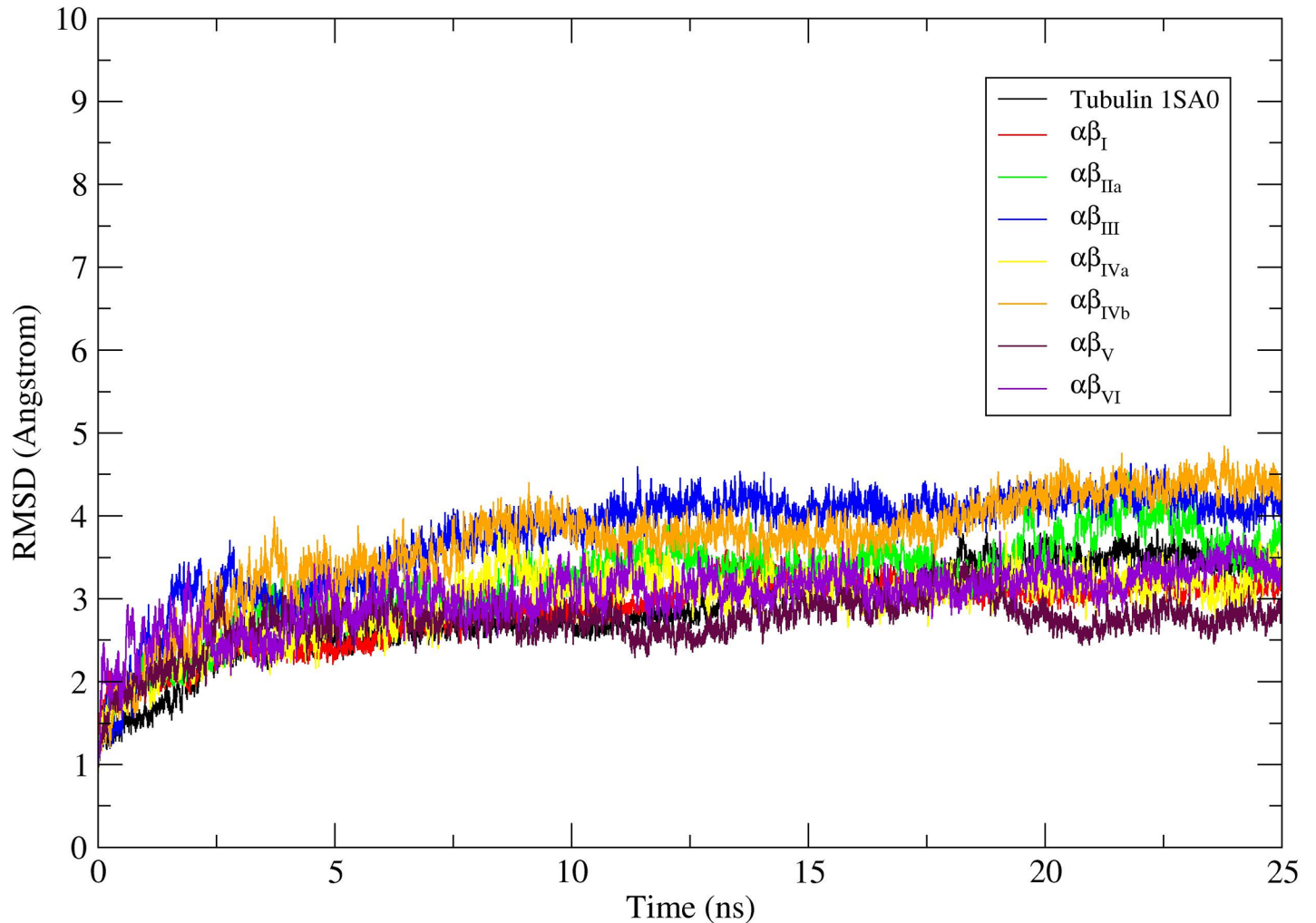


**Fig 4. Root mean square deviations (RMSD) corresponding to tubulin 1SA0 and  $\alpha\beta$ -tubulin isotypes.** RMSD correspond to tubulin 1SA0 (black color),  $\alpha\beta$ I (red color),  $\alpha\beta$ IIa (green color),  $\alpha\beta$ III (blue color),  $\alpha\beta$ IVa (yellow color),  $\alpha\beta$ IVb (orange color),  $\alpha\beta$ V (maroon color), and  $\alpha\beta$ VI (violet color) tubulin heterodimer for 25ns molecular dynamics simulations.

<https://doi.org/10.1371/journal.pone.0194934.g004>

indanocine complex (Fig 5B) shows that the hydrogen bonding interaction of indanocine occurs with only  $\alpha$ -tubulin residue Pro-222(1.88Å), Val-177 (2.90Å) as well as with O<sub>3</sub>P of GTP (1.81Å) (Table 2). In the  $\alpha\beta$ I tubulin, indanocine is expelled from the binding pocket and moves towards the surface of  $\alpha\beta$ -tubulin interface (S1 Movie). Here, the dimethoxyaniline group of indanocine interacts with Pro-222 and Val-177 of  $\alpha$ -tubulin whereas the dimethylphenol group interacts with the O<sub>3</sub>P atom of GTP (S11B Fig and Table 2).

The MD simulated  $\alpha\beta$ IIa-indanocine complex (Fig 5C) shows the hydrogen bonding interaction (Table 2) of indanocine with residues Asn-256 (2.80Å), Asn-256(2.96Å) and Leu-246 (3.03Å) of  $\beta$ -tubulin, and Lys-252(2.68Å), Asn-101(1.81Å) and Ala-180(2.99Å) of  $\alpha$ -tubulin (S11C Fig). Here, the residues Leu-246, Lys-252, Asn-256, Asn-101 and Ala-180 interact with dimethoxyaniline group of indanocine (S11C Fig). Further, in the  $\alpha\beta$ III-indanocine complex (Fig 5D), indanocine makes interactions with Val-349(2.71Å), Asn-247 (2.50Å), Asn-247 (2.36Å), and Asp-249(1.90Å) as well as with O<sub>3</sub>P of GTP (2.07Å) (Table 2). Here, Val-349 interacts with the dimethylphenol group and O<sub>3</sub>P of GTP, Asn-247 and Asp-248 interact with

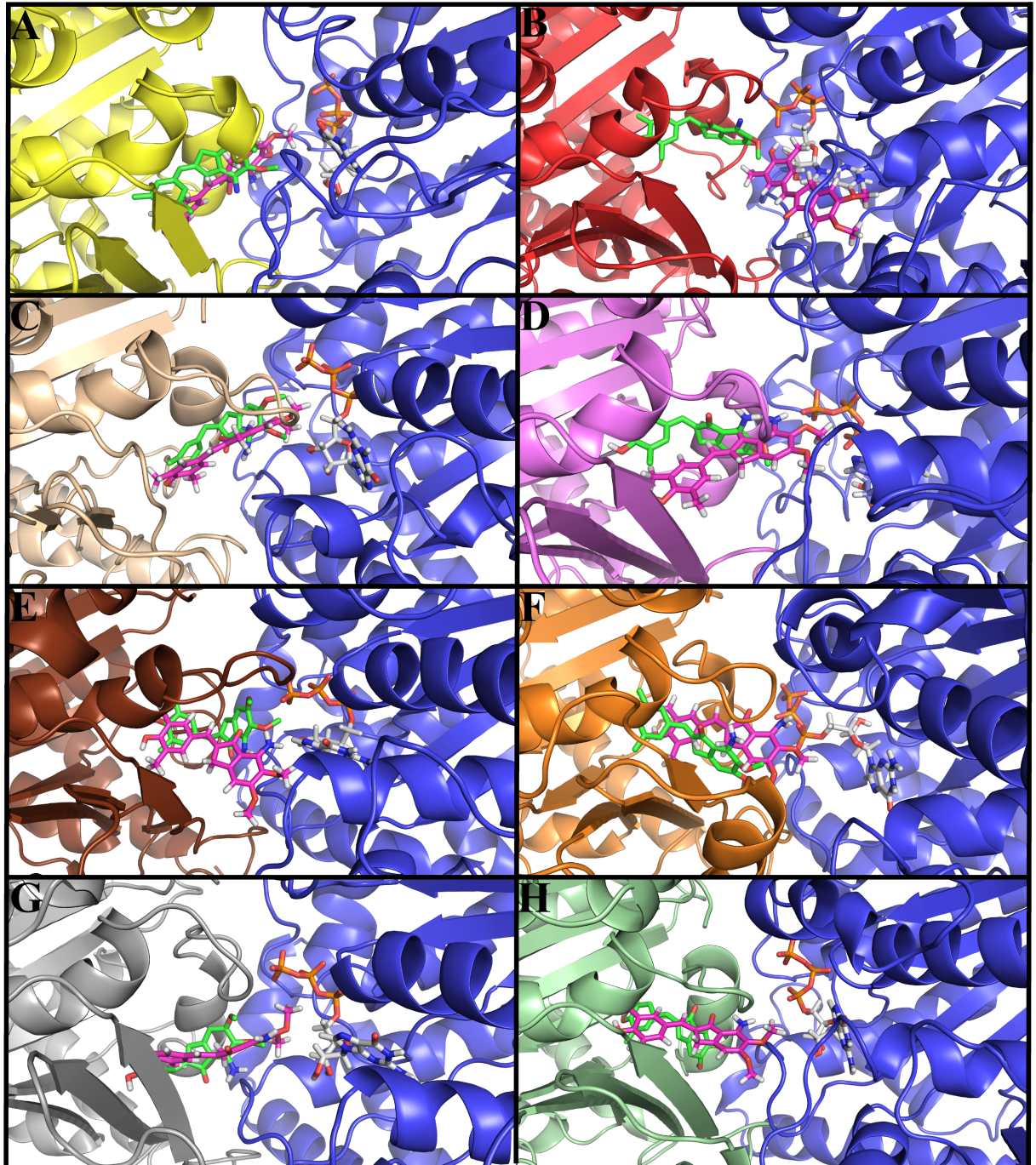


**Fig 5. Molecular dynamics simulated structures of  $\alpha\beta$  tubulin isotypes-indanocine complex.** The position of indanocine before and after the simulation is shown for comparison. The color scheme for  $\alpha\beta$ -tubulin is same as shown in Fig 3. The color scheme for initial docked conformation of indanocine (before MD simulation) shown in green color while indanocine after MD simulation is shown in magenta color. (A) Tubulin1SA0-indanocine complex (B)  $\alpha\beta$ I tubulin isotype-indanocine complex. (C)  $\alpha\beta$ IIa tubulin isotype-indanocine complex (D)  $\alpha\beta$ III tubulin isotype-indanocine complex (E)  $\alpha\beta$ IVa tubulin isotype-indanocine complex (F)  $\alpha\beta$ IVb tubulin isotype-indanocine complex (G)  $\alpha\beta$ V tubulin isotype-indanocine complex. (H)  $\alpha\beta$ VI tubulin isotype-indanocine complex.

<https://doi.org/10.1371/journal.pone.0194934.g005>

the dimethoxyaniline group of indanocine (S11D Fig). Analysis of the MD simulated average structure of  $\alpha\beta$ IVa-indanocine (Fig 5E) complex shows that indanocine makes interactions

**Table 2. RMSD and hydrogen bonding interactions of different  $\alpha\beta$ -tubulin isotypes with indanocine after molecular dynamics simulation.**

Tubulin Isotypes	RMSD after MD	Hydrogen bonding interactions			Figure reference
		Atoms involved	Distance (Å)	Angle (Degree)	
tubulin 1SA0	4.11	Cys-239-S...HC-Ind	3.00	163.80	<a href="#">Fig 5A, S11A Fig</a>
		Lys-350-CH...O-Ind	2.28	118.39	
		Asn-256-CH...O-Ind	2.82	115.36	
		Lys-252-CH...O-Ind	2.77	152.67	
		Asn-101-O...HC-Ind	2.91	163.50	
$\alpha\beta$ I	13.26	Thr-179-O...HN-Ind	1.86	162.50	<a href="#">Fig 5B, S11B Fig</a>
		Pro-222-O...HN-Ind	1.88	172.56	
		Val-177-CH...O-Ind	2.90	161.7	
$\alpha\beta$ Ia	2.92	GTP-O <sub>3</sub> P...HO-Ind	1.81	142.74	<a href="#">Fig 5C, S11C Fig</a>
		Asn256-NH...O-Ind	2.80	157.53	
		Asn256-NH...N-Ind	2.96	142.01	
		Lys252-CH...N-Ind	2.68	143.25	
		Leu246-O.....HC-Ind	3.03	146.82	
$\alpha\beta$ III	8.98	Ala-180-HC...N-Ind	2.99	147.80	<a href="#">Fig 5D, S11D Fig</a>
		Asn-101-CH...O-Ind	1.81	163.62	
		Val-349-O...HC-Ind	2.71	110.00	
		Asn-247-O...HC-Ind	2.50	114.10	
		Asn-247-NH...O-Ind	2.36	142.57	
$\alpha\beta$ IVa	5.92	Asp-249-NH...O-Ind	1.90	172.51	<a href="#">Fig 5E, S11E Fig</a>
		Ind-NH...O <sub>3</sub> P-GTP	2.07	154.18	
		Lys-252-CH...O-Ind	2.36	146.74	
		Lys-252-NH...O-Ind	2.90	121.73	
$\alpha\beta$ IVb	6.16	Val-180-CH...O-Ind	2.60	129.0	<a href="#">Fig 5F, S11F Fig</a>
		Ind-NH...N-GTP	2.13	163.38	
		Cys-239-SH...O-Ind	2.39	158.87	
		Lys-252-NH...O-Ind	1.93	149.29	
		Thr-351-O...HC-Ind	2.71	114.70	
$\alpha\beta$ V	4.63	Ind-NH...O <sub>1</sub> P-GTP	1.85	166.31	<a href="#">Fig 5G, S11G Fig</a>
		Lys-350-NH..O <sub>2</sub> P-GTP	1.73	156.19	
		Ala-315-O...HC-Ind	2.90	133.40	
		Thr-351-O...HC-Ind	2.91	124.40	
		Leu-246-CH...O-Ind	2.49	130.22	
$\alpha\beta$ VI	8.38	Asn-101-NH...O-Ind	2.35	134.81	<a href="#">Fig 5H, S11H Fig</a>
		Ind-O...HC6-GTP	2.70	115.20	
		Val-236-O...HO-Ind	2.06	129.91	
		Thr-315-O...HC-Ind	3.00	142.70	
		Asp-249-NH...O-Ind	2.59	159.19	
		Ser-178-NH—O-Ind	2.10	156.21	
		Ser-178-O...HN-Ind	2.17	153.87	
		Arg221-NH.....O-Ind	2.15	135.47	

<https://doi.org/10.1371/journal.pone.0194934.t002>

with Lys-252(2.36Å), Lys-252(2.90Å) of  $\beta$ -tubulin and Val-180(2.60Å) and adenosine of GTP (2.13Å) (Table 2). Lys-252, Val-180, and GTP interact with the dimethoxyaniline group of indanocine (S11E Fig). In the  $\alpha\beta$ IVa-indanocine complex (Fig 5E), indanocine is expelled from the  $\alpha\beta$ -tubulin interface, as the T7-loop moves backward and B9 sheet and a T5 loop of

$\alpha$ -tubulin also undergoes conformational changes which make enough space for indanocine to get expelled from the interface cavity (S5 Movie).

In the  $\alpha\beta$ IVb-indanocine MD simulated complex (Fig 5F), indanocine shows hydrogen bonding interactions with residues Cys-239(2.39Å), Lys-252(1.93Å), Lys-350(1.73Å), and Thr-351 (2.71Å) and O<sub>1</sub>P of GTP (1.85Å) (Table 2). Cys-239 interacts with the dimethylphenol group of indanocine whereas Lys-252, Lys-350, and Thr-351 of  $\beta$ -tubulin and O<sub>2</sub>P of GTP interact with the dimethoxyaniline group of indanocine (S11F Fig). Next, the analysis of  $\alpha\beta$ V-indanocine MD simulated complex (Fig 5G) shows that, indanocine forms hydrogen bonding interactions with the residues Ala-315(2.90Å), Thr-351(2.91Å), Leu-246 (2.49Å) of  $\beta$ -tubulin, and Asn-101(2.35Å) of  $\alpha$ -tubulin as well as with the HC6 of GTP(2.70Å) (Table 2). Here, Ala-315 interact with the dimethylphenol group of indanocine and Thr-351, Leu-246, Asn-101, and GTP interact with the dimethoxyaniline group of indanocine (S11G Fig). Finally, the analysis of  $\alpha\beta$ VI-indanocine (Fig 5H) complex shows hydrogen bonding interactions between indanocine with residues Val-236(2.06Å), Thr-315(3.00Å), Asp-249(2.59Å) of  $\beta$ -tubulin, and Ser-178(2.10Å), Ser-178(2.17Å) and Arg-221(2.15Å) of  $\alpha$ -tubulin (Table 2). Here, Val-236 and Thr-315 interact with the dimethylphenol group of indanocine and Ser-178, and Arg-221 and Asp-249 interact with the dimethoxyaniline group of indanocine (S11H Fig).

The analysis of molecular dynamics simulated average structures of different  $\alpha\beta$ -tubulin-indanocine complexes shows that the dimethoxyaniline group of indanocine interacts with  $\alpha$ -tubulin and  $\beta$ -tubulin residues, while the dimethylphenol group of indanocine interacts with  $\beta$ -tubulin residues except in case of only  $\alpha\beta$ I-indanocine complex. In  $\alpha\beta$ I-indanocine complex, indanocine is expelled from its initial binding pose and moves towards the surface of  $\alpha$ -tubulin (S2 Movie). Overall, the residues at the indanocine binding pocket such as Cys-239, Leu-246, Lys-252, Ala-315, Lys-350 and Thr-351 of  $\beta$ -tubulin, and Asn-101, Ser-178, Thr-179, Val-180 of T5-loop of  $\alpha$ -tubulin play an important role in the binding of indanocine at the interface of  $\alpha\beta$ -tubulin isotypes. However, the  $\alpha\beta$ I-indanocine complex does not show any such bonding interactions, as indanocine moves from its initial binding position (Table 2 and S2 Movie). In tubulin 1SA0 and human tubulin isotypes  $\alpha\beta$ IIa,  $\alpha\beta$ III,  $\alpha\beta$ IVb,  $\alpha\beta$ V, and  $\alpha\beta$ VI, the T7 loop of  $\beta$ -tubulin move forward and the B9-sheet of  $\beta$ -tubulin and T5 loop of  $\alpha$ -tubulin move backward, which makes enough space to adopt indanocine at the  $\alpha\beta$ -interface cavity (S1 Movie, S3 and S4 Movies, S6–S8 Movies). Further, we calculated the electrostatic potentials to show the binding mode of indanocine after molecular dynamics simulation (S12A–S12H Fig). The electrostatic potential surface shows that indanocine is located inside the binding cavity of human  $\beta$ -tubulin isotypes except in  $\beta$ I-tubulin (S12B Fig). Similar to hydrogen bonding interactions, the electrostatic and van der Waals interactions also play a role in the protein-ligand complex stabilization. Therefore, the MM-GBSA binding free energy calculations were used to further analyze the binding free energy difference between different  $\alpha\beta$ -tubulin isotype-indanocine complexes.

## Binding energy calculations

As reported earlier [10], the binding free energies for different  $\alpha\beta$ -tubulin isotypes with indanocine were calculated ignoring the entropic contribution to the binding free energy (Table 3). The estimated binding free energies ( $\Delta E_{\text{bind}}$ ) of tubulin 1SA0 and different  $\alpha\beta$ I,  $\alpha\beta$ IIa,  $\alpha\beta$ III,  $\alpha\beta$ IVa,  $\alpha\beta$ IVb,  $\alpha\beta$ V, and  $\alpha\beta$ VI tubulin isotypes with indanocine are -49.90, -41.39, -44.03, -43.47, -41.50, -44.57, -42.97, and -50.70 kcal/mol, respectively (Table 3). The  $\alpha\beta$ VI has the highest binding free energy for indanocine, whereas  $\alpha\beta$ I has the lowest binding free energy among the other  $\alpha\beta$ -tubulin isotypes. The binding free energy decreases in the order of  $\alpha\beta$ VI >  $\alpha\beta$ IIb >  $\alpha\beta$ IVb >  $\alpha\beta$ IIa >  $\alpha\beta$ III >  $\alpha\beta$ V >  $\alpha\beta$ IVa >  $\alpha\beta$ I. The lower binding free energy

**Table 3. Binding energy of different  $\alpha\beta$ -tubulin isotypes with indanocine.**

Tubulin isotypes	$\Delta E_{vdw}$	$\Delta E_{ele}$	$\Delta E_{gas}$	$\Delta E_{sol}$	$^a\Delta E_{bind}$
tubulin 1SA0	-56.85	-19.20	-76.05	26.15	-49.90
$\alpha\beta$ I	-42.26	-34.22	-76.48	35.09	-41.39
$\alpha\beta$ IIa	-46.27	-24.74	-71.01	26.98	-44.03
$\alpha\beta$ III	-47.10	-19.74	-66.84	23.37	-43.47
$\alpha\beta$ IVa	-46.22	-10.93	-57.15	15.65	-41.50
$\alpha\beta$ IVb	-47.66	-23.58	-71.24	26.67	-44.57
$\alpha\beta$ V	-51.06	-4.81	-55.87	12.90	-42.97
$\alpha\beta$ VI	-52.21	-20.99	-73.20	22.50	-50.70

$$^a\Delta E_{bind} = \Delta E_{gas} + \Delta E_{sol} = (\Delta E_{vdw} + \Delta E_{ele}) + (\Delta E_{polar} + \Delta E_{nonpolar})$$

<https://doi.org/10.1371/journal.pone.0194934.t003>

of indanocine for  $\alpha\beta$ I-tubulin isotype is due to maximum residue changes in the binding pocket of  $\beta$ I-tubulin such as Val236-Ile, Cys239-Ser, Ala315-Cys, Val316-Ile, and Thr351-Val as compared to other tubulin isotypes (Fig 2). However, indanocine exhibits a good binding affinity for  $\alpha\beta$ VI,  $\alpha\beta$ IIb,  $\alpha\beta$ IVb,  $\alpha\beta$ IIa,  $\alpha\beta$ III, and  $\alpha\beta$ V (Table 3). The van der Waal ( $\Delta E_{vdw}$ ) and electrostatic ( $\Delta E_{ele}$ ) interactions are important for the binding of the protein-ligand complex. Here, van der Waal interactions make the highest contribution towards the binding free energy (Table 3), while the solvation energy ( $E_{sol}$ ) is unfavorable for binding of ligand. The  $\alpha\beta$ I-tubulin isotype shows the lowest van der Waals interaction energy in comparison to the other  $\alpha\beta$ -tubulin isotype-indanocine complexes. The net binding free energy is decided by a competition between  $E_{gas}$  and  $E_{sob}$ , and is the lowest for  $\alpha\beta$ I-tubulin isotype (Table 3).

## Conclusion

In this study, the binding affinity of indanocine with tubulin 1SA0 and seven human tubulin isotypes  $\alpha\beta$ I,  $\alpha\beta$ IIa,  $\alpha\beta$ III,  $\alpha\beta$ IVa,  $\alpha\beta$ IVb,  $\alpha\beta$ V, and  $\alpha\beta$ VI was investigated using sequence analysis, homology modeling, molecular docking, molecular dynamics simulations and binding free energy calculations. The residue compositions were found to be different at the indanocine binding pocket of human  $\beta$ I,  $\beta$ IIa,  $\beta$ III and  $\beta$ VI tubulin isotypes, whereas no such differences were found in the  $\beta$ IVa,  $\beta$ IVb and  $\beta$ V tubulin isotypes.

Further, molecular docking results show that indanocine prefers to bind at the interface of all  $\alpha\beta$ -tubulin isotypes i.e. at the colchicine binding site, as observed in the previous experimental study [21]. Indanocine shows different binding mode and binding energy for different  $\alpha\beta$ -tubulin isotypes; this might be due to the residue composition changes in and around the binding pocket of  $\beta$ -tubulin isotypes. The residues in the H7-Helix (Cys-239, Ile-236), T7-loop (Leu-246, Ala-248), H8-helix (Lys-252, Asn-256) and B9-sheet (Lys-350) of  $\beta$ -tubulin and T5-loop (Ser-178, Thr-179, Val-180) of  $\alpha$ -tubulin are involved in the hydrogen bonding interactions with indanocine.

Molecular dynamics simulations were performed on  $\alpha\beta$ -tubulin isotype-indanocine docked complexes, to further investigate the effect of residue composition differences on the binding of indanocine. Our molecular dynamics simulations results show that indanocine is completely adopted inside the binding pocket of tubulin 1SA0 and  $\alpha\beta$ IIa,  $\alpha\beta$ III,  $\alpha\beta$ IVb,  $\alpha\beta$ V and  $\alpha\beta$ VI tubulin isotypes, whereas it is expelled from the interface of  $\alpha\beta$ I, and  $\alpha\beta$ IVa-tubulin isotype. Here, the T7-loop of  $\beta$ -tubulin moves backward; meanwhile the B9 sheet of  $\beta$ -tubulin and T5-loop of  $\alpha$ -tubulin shows conformational change. This leads to making an ample space at the interface of  $\alpha\beta$ I, and  $\alpha\beta$ IVa tubulin isotypes which is helpful to expel indanocine from the interface cavity. Whereas in case of other  $\alpha\beta$ -tubulin isotypes-indanocine complexes, the T7 loop moves forward

which helps to adopt indanocine at the binding pocket. Further, binding free energy calculations show that the tubulin isotypes  $\alpha\beta$ Ia,  $\alpha\beta$ III,  $\alpha\beta$ IVa,  $\alpha\beta$ IVb,  $\alpha\beta$ V and  $\alpha\beta$ VI have the highest binding free energy and  $\alpha\beta$ I-tubulin isotype has the lowest binding free energy for indanocine. One of the reasons behind the less binding free energy of  $\alpha\beta$ I-tubulin isotype toward indanocine might be due to maximum residue changes at the binding site.

Thus, our present computational study provides a detailed understanding of the molecular interactions of human  $\alpha\beta$ -tubulin isotypes with indanocine and provides insight for designing superior indanocine analogues with isotype specificity. These superior analogues can be valuable in the treating patients with advanced carcinomas which exhibit tubulin isotype specificity or can be helpful in developing personalized medicines for cancer patients.

## Supporting information

**S1 Text. Stereo-chemical Quality Analysis of different  $\alpha\beta$ -tubulin isotypes.**  
(DOC)

**S1 Fig. PROCHECK plot for tubulin 1SA0.**  
(PDF)

**S2 Fig. PROCHECK plot for  $\alpha\beta$ I-tubulin isotypes.**  
(PDF)

**S3 Fig. PROCHECK plot for  $\alpha\beta$ Ia-tubulin isotypes.**  
(PDF)

**S4 Fig. PROCHECK plot for  $\alpha\beta$ III-tubulin isotypes.**  
(PDF)

**S5 Fig. PROCHECK plot for  $\alpha\beta$ IVa-tubulin isotypes.**  
(PDF)

**S6 Fig. PROCHECK plot for  $\alpha\beta$ IVb-tubulin isotypes.**  
(PDF)

**S7 Fig. PROCHECK plot for  $\alpha\beta$ V-tubulin isotypes.**  
(PDF)

**S8 Fig. PROCHECK plot for  $\alpha\beta$ VI-tubulin isotypes.**  
(PDF)

**S9 Fig. Hydrogen bonding interactions of indanocine with different  $\alpha\beta$ -tubulin isotypes after molecular docking.** (A) Tubulin 1SA0 and indanocine complex, indanocine interacts with Ala-315 (2.18Å), Lys-350 (2.10Å) of  $\beta$ -tubulin, and Thr-179 (2.16Å) and Asn-101 (2.63Å) of  $\alpha$ -tubulin (B)  $\alpha\beta$ I-tubulin and indanocine complex, indanocine interacts with Ile-236 (2.22Å), Leu-246(2.00Å), Leu-246(2.14Å), Lys-252 (2.54Å) of  $\beta$ -tubulin, and Asn-101(2.92Å) of  $\alpha$ -tubulin (C)  $\alpha\beta$ Ia tubulin isotype and indanocine complex, here indanocine interacts with Lys-252(2.42Å), and Lys-350(1.90Å) of  $\beta$ -tubulin, and with Thr-179(1.98Å) and Asn-101 (2.88Å) of T5-loop of  $\alpha$ -tubulin (D)  $\alpha\beta$ III tubulin isotype and indanocine complex, indanocine interacts with Leu-246 (2.10Å), Lys-252(2.61Å) and Tyr-169(2.00Å) of  $\beta$ -tubulin (E)  $\alpha\beta$ IVa tubulin isotype and indanocine complex, indanocine interacts with Cys-239 (1.84Å), Lys-252 (2.07Å) of  $\beta$ -tubulin and Ser-178 (2.26Å) and Ser-178(2.20Å) of T5-loop of  $\alpha$ -tubulin (F)  $\alpha\beta$ IVb tubulin isotype and indanocine complex, indanocine interacts with residue Val-236 (1.73Å), Cys-239 (2.90Å), Leu-240 (2.38Å), Leu-246 (2.23Å), Ala-248(2.70Å) and Asn-256 (2.58Å) of  $\alpha$ -tubulin and Ser-178 (2.19Å) of T5-loop of  $\beta$ -tubulin (G)  $\alpha\beta$ V tubulin isotype and



indanocine complex, indanocine interacts with Ala-315 (1.88Å), Lys-252 (2.29Å) of  $\beta$ -tubulin, Asn-101 (2.17Å), and Val-180 (2.80Å) and Thr-179 (2.20Å) of  $\alpha$ -tubulin. and (H)  $\alpha\beta$ VI tubulin isotype and indanocine complex, indanocine interacts with Tyr-169 (2.06Å), Asn-256 (2.60Å) Lys-350 (2.72Å) and Lys-252 (1.97Å) of  $\beta$ -tubulin.

(TIF)

**S10 Fig. The electrostatic contact potential of different  $\beta$ -tubulin isotypes with docked indanocine.** The red, blue and white color represents the negative, positive and neutral electrostatic potentials, respectively. The indanocine bind at the interface of the cavity of  $\beta$ -tubulin in all the tubulin isotypes. indanocine is shown in green color; oxygen, nitrogen, and hydrogen atoms are shown in red, blue, and grey colors respectively. (A) Tubulin 1SA0 and indanocine complex (B)  $\beta$ I-tubulin and Indanocine complex (C)  $\beta$ IIa tubulin isotype and indanocine complex, (D)  $\beta$ III tubulin isotype and indanocine complex (E)  $\beta$ IVa tubulin isotype and indanocine complex (F)  $\beta$ IVb tubulin isotype and indanocine complex (G)  $\beta$ V tubulin isotype and indanocine complex and (H)  $\beta$ VI tubulin isotype and indanocine complex.

(TIF)

**S11 Fig. Hydrogen bonding interactions of indanocine with different  $\alpha\beta$ -tubulin isotypes after molecular dynamics simulation.** (A) Tubulin 1SA0 and indanocine complex, indanocine shows interaction with Cys-239(3.00Å), Lys-350(2.28Å), Lys-252 (2.77Å), and Asn-256 (2.82Å) of  $\beta$ -tubulin and Asn-101(2.91Å) and Thr-179(1.86Å) of  $\alpha$ -tubulin (B)  $\alpha\beta$ I-tubulin and indanocine complex, indanocine shows interaction with Pro-222(1.88Å), Val-177 (2.90Å) as well as with O<sub>3</sub>P of GTP(1.81Å) (C)  $\alpha\beta$ IIa tubulin isotype and indanocine complex, indanocine shows interaction with Asn-256 (2.80Å), Asn-256(2.96Å) and Leu-246(3.03Å) of  $\beta$ -tubulin, and Lys-252(2.68Å), Asn-101(1.81Å) and Ala-180(2.99Å) of  $\alpha$ -tubulin (D)  $\alpha\beta$ III tubulin isotype and indanocine complex, indanocine shows interaction with Val-349(2.71Å), Asn-247 (2.50Å), Asn-247(2.36Å), and Asp-249(1.90Å) as well as with O<sub>3</sub>P of GTP (2.07Å) (E)  $\alpha\beta$ IVa tubulin isotype and indanocine complex, indanocine shows interaction with Lys-252(2.36Å), Lys-252(2.90Å) of  $\beta$ -tubulin and Val-180(2.60Å) and adenosine of GTP (2.13Å) (F)  $\alpha\beta$ IVb tubulin isotype and indanocine complex, indanocine shows interaction with Cys-239(2.39Å), Lys-252(1.93Å), Lys-350(1.73Å), and Thr-351 (2.71Å) and O<sub>1</sub>P of GTP (1.85Å) (G)  $\alpha\beta$ V tubulin isotype and indanocine complex, indanocine shows interaction with Ala-315(2.90Å), Thr-351(2.91Å), Leu-246 (2.49Å) of  $\beta$ -tubulin, and Asn-101(2.35Å) of  $\alpha$ -tubulin as well as with the HC6 of GTP(2.70Å) and (H)  $\alpha\beta$ VI tubulin isotype and indanocine complex, indanocine shows interaction with Val-236(2.06Å), Thr-315(3.00Å), Asp-249(2.59Å) of  $\beta$ -tubulin, and Ser-178(2.10Å), Ser-178(2.17Å) and Arg-221(2.15Å) of  $\alpha$ -tubulin.

(TIF)

**S12 Fig. The electrostatic contact potential of indanocine with different  $\beta$ -tubulin isotypes after molecular dynamics simulation.** Colour scheme is same as shown in S2 Fig. (A) Tubulin 1SA0 and indanocine complex (B)  $\beta$ I-tubulin and Indanocine complex, here indanocine expelled from the binding pocket (C)  $\beta$ IIa tubulin isotype and indanocine complex, (D)  $\beta$ III tubulin isotype and indanocine complex (E)  $\beta$ IVa tubulin isotype and indanocine complex (F)  $\beta$ IVb tubulin isotype and indanocine complex (G)  $\beta$ V tubulin isotype and indanocine complex and (H)  $\beta$ VI tubulin isotype and indanocine complex.

(TIF)

**S1 Movie. MD simulation movie of tubulin 1SA0 and indanocine.**

(MPG)

**S2 Movie. MD simulation movie of  $\alpha\beta$ I and indanocine.**

(MPG)

**S3 Movie. MD simulation movie of  $\alpha\beta$ IIa tubulin isotype and indanocine.**

(MPG)

**S4 Movie. MD simulation movie of  $\alpha\beta$ III tubulin isotype and indanocine.**

(MPG)

**S5 Movie. MD simulation movie of  $\alpha\beta$ IVa and indanocine.**

(MPG)

**S6 Movie. MD simulation movie of  $\alpha\beta$ IVb tubulin isotype and indanocine.**

(MPG)

**S7 Movie. MD simulation movie of  $\alpha\beta$ V tubulin isotype and indanocine.**

(MPG)

**S8 Movie. MD simulation movie of  $\alpha\beta$ VI tubulin isotype and indanocine.**

(MPG)

## Author Contributions

**Conceptualization:** Bajarang Vasant Kumbhar, Dulal Panda, Ambarish Kunwar.**Data curation:** Bajarang Vasant Kumbhar.**Formal analysis:** Bajarang Vasant Kumbhar, Ambarish Kunwar.**Funding acquisition:** Ambarish Kunwar.**Investigation:** Bajarang Vasant Kumbhar, Ambarish Kunwar.**Methodology:** Bajarang Vasant Kumbhar, Dulal Panda, Ambarish Kunwar.**Project administration:** Ambarish Kunwar.**Resources:** Ambarish Kunwar.**Software:** Dulal Panda, Ambarish Kunwar.**Supervision:** Dulal Panda, Ambarish Kunwar.**Validation:** Ambarish Kunwar.**Writing – original draft:** Bajarang Vasant Kumbhar, Dulal Panda, Ambarish Kunwar.**Writing – review & editing:** Bajarang Vasant Kumbhar, Dulal Panda, Ambarish Kunwar.

## References

1. Valiron O, Caudron N, Job D. Microtubule dynamics. Cellular and molecular life sciences: CMLS. 2001; 58: 2069–2084. <https://doi.org/10.1007/PL00000837> PMID: 11814057
2. Ludueña RF. Multiple forms of tubulin: different gene products and covalent modifications. International review of cytology. 1998; 178: 207–275. [https://doi.org/10.1016/S0074-7696\(08\)62138-5](https://doi.org/10.1016/S0074-7696(08)62138-5) PMID: 9348671
3. Ludueña RF, Banerjee A. The Isotypes of Tubulin. The Role of Microtubules in Cell Biology, Neurobiology, and Oncology. 2008. pp. 123–175. [https://doi.org/10.1007/978-1-59745-336-3\\_6](https://doi.org/10.1007/978-1-59745-336-3_6)
4. Ludueña RF. Are tubulin isotypes functionally significant. Molecular Biology of the Cell. 1993; 4: 445–457. <https://doi.org/10.1091/mbc.4.5.445> PMID: 8334301
5. Kavallaris M. Microtubules and resistance to tubulin-binding agents. Nature reviews Cancer. 2010; 10: 194–204. <https://doi.org/10.1038/nrc2803> PMID: 20147901

6. Panda D, Miller HP, Banerjee a, Ludueña RF, Wilson L. Microtubule dynamics in vitro are regulated by the tubulin isotype composition. *Proceedings of the National Academy of Sciences of the United States of America*. 1994; 91: 11358–11362. <https://doi.org/10.1073/pnas.91.24.11358> PMID: 7972064
7. Pamula MC, Ti SC, Kapoor TM. The structured core of human  $\beta$  tubulin confers isotype-specific polymerization properties. *Journal of Cell Biology*. 2016; 213: 425–433. <https://doi.org/10.1083/jcb.201603050> PMID: 27185835
8. Vemu A, Atherton J, Spector JO, Moores CA, Roll-Mecak A. Tubulin isoform composition tunes microtubule dynamics. *Molecular biology of the cell*. 2017; <https://doi.org/10.1091/mbc.E17-02-0124> PMID: 29021343
9. Dumontet C, Sikic BI. Mechanisms of Action of and Resistance to Antitubulin Agents: Microtubule Dynamics, Drug Transport, and Cell Death. *Journal of Clinical Oncology*. 1999; 17: 1061–1061. <https://doi.org/10.1200/JCO.1999.17.3.1061> PMID: 10071301
10. Kumbhar BV, Borogaon A, Panda D, Kunwar A. Exploring the Origin of Differential Binding Affinities of Human Tubulin Isotypes  $\alpha\beta$ II,  $\alpha\beta$ III and  $\alpha\beta$ IV for DAMA-Colchicine Using Homology Modelling, Molecular Docking and Molecular Dynamics Simulations. *Plos One*. 2016; 11: e0156048. <https://doi.org/10.1371/journal.pone.0156048> PMID: 27227832
11. Parker AL, Teo WS, McCarroll JA, Kavallaris M. An Emerging Role for Tubulin Isotypes in Modulating Cancer Biology and Chemotherapy Resistance. *International Journal of Molecular Sciences*. 2017; 18: 1434. <https://doi.org/10.3390/ijms18071434> PMID: 28677634
12. Xu K, Schwarz PM, Ludueña RF. Interaction of nocodazole with tubulin isotypes. *Drug Development Research*. Wiley Subscription Services, Inc., A Wiley Company; 2002; 55: 91–96. <https://doi.org/10.1002/ddr.10023>
13. Banerjee A, Ludueña RF. Kinetics of colchicine binding to purified beta-tubulin isotypes from bovine brain. *The Journal of biological chemistry*. 1992; 267: 13335–9. Available: <http://www.jbc.org/content/267/19/13335>. PMID: 1618835
14. Ohishi Y, Oda Y, Basaki Y, Kobayashi H, Wake N, Kuwano M, et al. Expression of beta-tubulin isotypes in human primary ovarian carcinoma. *Gynecologic Oncology*. 2007; 105: 586–592. <https://doi.org/10.1016/j.ygyno.2007.01.044> PMID: 17343904
15. Kavallaris M, Kuo DY, Burkhart CA, Regl DL, Norris MD, Haber M, et al. Taxol-resistant epithelial ovarian tumors are associated with altered expression of specific beta-tubulin isotypes. *The Journal of clinical investigation*. 1997; 100: 1282–1293. <https://doi.org/10.1172/JCI119642> PMID: 9276747
16. Christoph DC, Kasper S, Gauler TC, Loesch C, Engelhard M, Theegarten D, et al.  $\beta$ V-tubulin expression is associated with outcome following taxane-based chemotherapy in non-small cell lung cancer. *British journal of cancer*. 2012; 107: 823–30. <https://doi.org/10.1038/bjc.2012.324> PMID: 22836512
17. Ranganathan S, Benetatos C a, Colarusso PJ, Dexter DW, Hudes GR. Altered beta-tubulin isotype expression in paclitaxel-resistant human prostate carcinoma cells. *British journal of cancer*. 1998; 77: 562–566. PMID: 9484812
18. Derry WB, Wilson L, Khan IA, Ludueña RF, Jordan MA. Taxol Differentially Modulates the Dynamics of Microtubules Assembled from Unfractionated and Purified  $\beta$ -Tubulin Isotypes. *Biochemistry*. 1997; 36: 3554–3562. <https://doi.org/10.1021/bi962724m> PMID: 9132006
19. Leoni LM, Hamel E, Genini D, Shih H, Carrera CJ, Cottam HB, et al. Indanocine, a microtubule-binding indanone and a selective inducer of apoptosis in multidrug-resistant cancer cells. *Journal of the National Cancer Institute*. 2000; 92: 217–224. <https://doi.org/10.1093/jnci/92.3.217> PMID: 10655438
20. Kapoor S, Panda D. Kinetic stabilization of microtubule dynamics by indanocine perturbs EB1 localization, induces defects in cell polarity and inhibits migration of MDA-MB-231 cells. *Biochemical Pharmacology*. 2012; 83: 1495–1506. <https://doi.org/10.1016/j.bcp.2012.02.012> PMID: 22387536
21. Das L, Gupta S, Dasgupta D, Poddar A, Janik ME, Bhattacharyya B. Binding of indanocine to the colchicine site on tubulin promotes fluorescence, and its binding parameters resemble those of the colchicine analogue AC. *Biochemistry*. 2009; 48: 1628–1635. <https://doi.org/10.1021/bi801575e> PMID: 19182899
22. Goujon M, McWilliam H, Li W, Valentin F, Squizzato S, Paern J, et al. A new bioinformatics analysis tools framework at EMBL-EBI. *Nucleic Acids Research*. 2010; 38. <https://doi.org/10.1093/nar/gkq313> PMID: 20439314
23. Ravelli RBG, Gigant B, Curmi PA, Jourdain I, Lachkar S, Sobel A, et al. Insight into tubulin regulation from a complex with colchicine and a stathmin-like domain. *Nature*. 2004; 428: 198–202. <https://doi.org/10.1038/nature02393> PMID: 15014504
24. Sali A, Blundell TL. Comparative protein modelling by satisfaction of spatial restraints. *Journal of molecular biology*. 1993; 234: 779–815. <https://doi.org/10.1006/jmbi.1993.1626> PMID: 8254673

25. Luchko T, Torin Huzil J, Stepanova M, Tuszynski J. Conformational analysis of the carboxy-terminal tails of human  $\beta$ -tubulin isotypes. *Biophysical Journal*. 2008; 94: 1971–1982. <https://doi.org/10.1529/biophysj.107.115113> PMID: 17993481
26. Laskowski R a., MacArthur MW, Moss DS, Thornton JM. PROCHECK: a program to check the stereochemical quality of protein structures. *Journal of Applied Crystallography*. 1993; 26: 283–291. <https://doi.org/10.1107/S0021889892009944>
27. Colovos C, Yeates TO. Verification of protein structures: patterns of nonbonded atomic interactions. *Protein science: a publication of the Protein Society*. 1993; 2: 1511–1519. <https://doi.org/10.1002/pro.5560020916> PMID: 8401235
28. Case D.A., Darden T.A., Cheatham T.E. III, C L. Simmerling J. Wang R.E. Duke R, Luo R.C. Walker W. Zhang K.M. Merz B. Roberts S. Hayik A. Roitberg GS, Swails J., A W. Götz I. Kolossváry K.F. Wong F. Paesani J. Vanicek R.M. Wolf JL, Wu X., Brozell S.R., Steinbrecher T., Gohlke H., Cai Q., Ye X., Wang J., Hsieh M.-J. Cui G, Roe D.R., Mathews D.H., Seetin M.G., Salomon-Ferrer R., Sagui C., Babin V. Luchko T, Gusarov S., Kovalenko A. and PAK. AmberTools12 Reference Manual. AMBER 12, University of California, San Francisco. 2012.
29. Meagher KL, Redman LT, Carlson HA. Development of polyphosphate parameters for use with the AMBER force field. *Journal of Computational Chemistry*. 2003; 24: 1016–1025. <https://doi.org/10.1002/jcc.10262> PMID: 12759902
30. Allnér O, Nilsson L, Villa A. Magnesium ion-water coordination and exchange in biomolecular simulations. *Journal of Chemical Theory and Computation*. 2012; 8: 1493–1502. <https://doi.org/10.1021/ct3000734> PMID: 26596759
31. Morris GM, Ruth H, Lindstrom W, Sanner MF, Belew RK, Goodsell DS, et al. Software news and updates AutoDock4 and AutoDockTools4: Automated docking with selective receptor flexibility. *Journal of Computational Chemistry*. 2009; 30: 2785–2791. <https://doi.org/10.1002/jcc.21256> PMID: 19399780
32. Schüttelkopf AW, Van Aalten DMF. PRODRG: A tool for high-throughput crystallography of protein-ligand complexes. *Acta Crystallographica Section D: Biological Crystallography*. 2004; 60: 1355–1363. <https://doi.org/10.1107/S0907444904011679> PMID: 15272157
33. Rai A, Gupta TK, Kini S, Kunwar A, Surolia A, Panda D. CXI-benzo-84 reversibly binds to tubulin at colchicine site and induces apoptosis in cancer cells. *Biochemical Pharmacology*. 2013; 86: 378–391. <https://doi.org/10.1016/j.bcp.2013.05.024> PMID: 23747346
34. Venghateri JB, Gupta TK, Verma PJ, Kunwar A, Panda D. Ansamitocin P3 depolymerizes microtubules and induces apoptosis by binding to tubulin at the vinblastine site. *PloS one*. 2013; 8: e75182. <https://doi.org/10.1371/journal.pone.0075182> PMID: 24124473
35. Pandey RK, Kumbhar BV, Srivastava S, Malik R, Sundar S, Kunwar A, et al. Febrifugine analogues as *Leishmania donovani* trypanothione reductase inhibitors: binding energy analysis assisted by molecular docking, ADMET and molecular dynamics simulation. *Journal of Biomolecular Structure and Dynamics*. 2016; 1102: 1–49. <https://doi.org/10.1080/07391102.2015.1135298>
36. Chakraborti S, Chakravarty D, Gupta S, Chatterji BP, Dhar G, Poddar A, et al. Discrimination of ligands with different flexibilities resulting from the plasticity of the binding site in tubulin. *Biochemistry*. 2012; 51: 7138–7148. <https://doi.org/10.1021/bi300474q> PMID: 22891709
37. Tsui V, David A, Case DA. Molecular Dynamics Simulations of Nucleic Acids with a Generalized Born Solvation Model. *Journal of the American Chemical Society*. 2000; 122: 2489–2498. <https://doi.org/10.1021/ja9939385>
38. Humphrey W, Dalke A, Schulten K. VMD: Visual molecular dynamics. *Journal of Molecular Graphics*. 1996; 14: 33–38. [https://doi.org/10.1016/0263-7855\(96\)00018-5](https://doi.org/10.1016/0263-7855(96)00018-5) PMID: 8744570
39. DeLano WL. The PyMOL Molecular Graphics System, Version 1.1. Schrödinger LLC. 2002; <http://www.pymol.org>. 10.1038/hr.2014.17
40. Miller BR, McGee TD, Swails JM, Homeyer N, Gohlke H, Roitberg AE. MMPBSA.py: An efficient program for end-state free energy calculations. *Journal of Chemical Theory and Computation*. 2012; 8: 3314–3321. <https://doi.org/10.1021/ct300418h> PMID: 26605738